Coupling of a two phase gas liquid compositional 3D Darcy flow with a 1D compositional free gas flow

Konstantin Brenner, Roland Masson, Laurent Trenty, Yumeng Zhang

Coupling of a two phase gas liquid compositional 3D Darcy flow with a 1D compositional free gas flow

K. Brenner*, R. Masson†, L. Trenty‡, Y. Zhang§

October 27, 2015

Abstract

A model coupling a three dimensional gas liquid compositional Darcy flow and a one dimensional compositional free gas flow is presented. The coupling conditions at the interface between the gallery and the porous medium account for the molar normal fluxes continuity for each component, the gas liquid thermodynamical equilibrium, the gas pressure continuity and the gas and liquid molar fractions continuity. This model is applied to the simulation of the mass exchanges at the interface between the repository and the ventilation excavated gallery in a nuclear waste geological repository. The spatial discretization is essentially nodal and based on the Vertex Approximate Gradient (VAG) scheme. Compared with classical nodal approaches such as the Control Volume Finite Element method, the VAG scheme has the advantage to avoid the mixture of different material properties and models in the control volumes located at the interfaces. The discrete model is validated using a quasi analytical solution for the stationary state, and the convergence of the VAG discretization is analysed for a simplified model coupling the Richards approximation in the porous medium and the gas pressure equation in the gallery.

1 Introduction

Flow and transport processes in domains composed of a porous medium and an adjacent free-flow region appear in a wide range of industrial and environmental applications. This is in particular the case for radioactive waste deep geological repositories where such models must be used to predict the mass and energy exchanges occurring at the interface between the repository and the ventilation excavated galleries. Typically, in this example, the porous medium initially saturated with the liquid phase is dried by suction in the neighbourhood of the interface. To model such physical processes, one needs to account in the porous medium for the flow of the liquid and gas phases including the vaporization of the water component in the gas phase and the dissolution of the gaseous components in the liquid phase. In the gallery, a single phase gas free flow can be considered assuming that the liquid phase is instantaneously vaporized at the interface. This single phase gas free flow has to be compositional to account for the change of the relative humidity in the gallery which has a strong

*Laboratoire de Mathématiques J.A. Dieudonné, UMR 7351 CNRS, University Nice Sophia Antipolis, and team COFFEE, INRIA Sophia Antipolis Méditerranée, Parc Valrose 06108 Nice Cedex 02, France, konstantin.brenner@unice.fr

†Laboratoire de Mathématiques J.A. Dieudonné, UMR 7351 CNRS, University Nice Sophia Antipolis, and team COFFEE, INRIA Sophia Antipolis Méditerranée, Parc Valrose 06108 Nice Cedex 02, France, roland.masson@unice.fr

‡Andra, 1-7 rue Jean Monnet 92290 Chatenay-Malabry, France, laurent.trenty@andra.fr

§Laboratoire de Mathématiques J.A. Dieudonné, UMR 7351 CNRS, University Nice Sophia Antipolis, and team COFFEE, INRIA Sophia Antipolis Méditerranée, Parc Valrose 06108 Nice Cedex 02, France, yumeng.zhang@unice.fr

feedback on the liquid flow rate at the interface.

If many works have been performed to model and discretize the coupling of single phase Darcy and free flows (see the review [12]), there is very little work so far on the coupling of a two phase gas liquid compositional Darcy flow with a single phase compositional free flow. Such a coupled model has been recently proposed in [5, 14] using proper matching conditions at the interface between the porous medium and the free flow regions. This model will be the starting point of our work and will be simplified taking into account the physical characteristics of our problem focusing on the drying processes at the interface between the nuclear waste repository and the ventilation excavated gallery.

To obtain our simplified model, it is first assumed that the longitudinal dimensions of the galleries are large compared with their diameters allowing to reduce the model in the gallery to a 1D free flow. Considering the low Mach flow regime in the galleries, a classical compositional No Pressure Wave (NPW) 1D approximation of the Navier Stokes equations is used [17]. This model corresponds to the low Mach number limit of the 1D Navier Stokes equations. The matching conditions at the porous medium gallery interface proposed in [5, 14] will also be simplified taking into account the low permeability of the repository. In this case, it can be assumed that the gas pressure, and the gas molar fractions are both continuous at the interface. In addition, following [5, 14], the thermodynamical equilibrium between the gas and liquid phases is assumed to hold at the interface. These assumptions lead to our reduced model using a 3D two phase compositional Darcy flow in the porous medium coupled to a 1D compositional NPW gas flow.

This reduced model is formulated in terms of a single set of unknowns used both in the porous medium and in the gallery. This set of unknowns is based on the formulation introduced in [9, 10] for a two components model and extended to an arbitrary number of components in [4]. It uses the gas pressure (extended in the single liquid phase region), the liquid pressure (extended in the single gas phase region) and the component fugacities as set of primary unknowns. The main advantage of this formulation is to use a unique set of unknowns and of equations whatever the set of present phases. In our coupled model, this set of unknowns is also used at the interface to formulate the 1D NPW model in the gallery taking into account the matching conditions.

The discretization of our coupled model is based on the Vertex Approximated Gradient (VAG) scheme introduced in [1] for the single phase Darcy flow and in [3] for compositional Darcy flows. The VAG scheme is roughly speaking a finite volume nodal approximation. Its main advantage compared with typical nodal finite volume schemes such as Control Volume Finite Element (CVFE) methods [14] is to avoid the mixing of different material properties inside the control volumes. The VAG scheme is here extended to take into account the coupling with the 1D free gas flow. It will be seen to offer a natural framework to keep a single model in the control volumes corresponding to the nodes located at the interface between the porous medium and the gallery.

In order to validate our discretization, the solution obtained numerically is compared with a quasi analytical stationary solution derived from a simplified model. A very good match is obtained at convergence. Then, a more complex geological test case is presented including two rocktypes and an anisotropic permeability field. A more advanced model is also tested including on the gallery side a gas molar fraction at the interface and a normal diffusion term between the interface and the gallery modelling the concentration boundary layer in the spirit of [5], [15]. The previous model corresponds to the limit when the diffusion coefficient tends to infinity.

The convergence of the VAG discretization is also analysed mathematically using a simplified

model coupling the Richards approximation in the porous medium coupled with a single phase Darcy flow in the gallery with fixed composition. The convergence of the VAG scheme to a weak solution is proved by compactness arguments adapting the techniques used in [7, 6] and exploiting the two point flux approximation in the gallery. The main new difficulty is related to the non linear dependence between the liquid and gas pressure at the interface accounting for the thermodynamical equilibrium.

The outline of the article is the following: section 2 details our reduced 3D-1D coupled model and its formulation using a single set of unknowns corresponding to the gas pressure, the liquid pressure and the component fugacities. In section 3, the VAG discretisation is extended to our coupled model. The VAG fluxes are first derived using a linear coupled model problem. Then, our discrete model is assessed numerically in section 4 on three test cases including a comparison with a quasi analytical stationary solution. Finally, we prove in section 5 the convergence of the scheme to a weak solution for a simplified model.

2 Coupled Model

Let ω and $S \subset \omega$ be two simply connected domains of $\mathbb{R}^2$ and $\Omega = (0, L) \times (\omega \setminus \overline{S})$ be the cylindrical domain defining the porous medium. The curvilinear coordinate along ∂S will be denoted by s while x denotes the coordinate along $(0, L)$. The excavated gallery corresponds to the domain $(0, L) \times S$ and it is assumed that the free flow in the gallery depends only on the x coordinate along the gallery and on the time $t \in (0, T)$. Let us denote by $\Gamma = (0, L) \times \partial S$ the interface between the gallery and the porous medium, by $\Gamma_N = (\{0\} \times (\omega \setminus \overline{S})) \cup (\{L\} \times (\omega \setminus \overline{S}))$ and $\Gamma_D = ((0, L) \times \partial\omega)$ the remaining boundaries of Ω.

Let us denote by $1_{\partial S}$ the function equal to 1 on ∂S. In order to avoid heavy notations, we shall keep in the following the same notation for a function $v \in L^2(0, L)$ and its prolongation $v \otimes 1_{\partial S}$ in $L^2(\Gamma)$. Likewise, for any function $u \in L^2(\Gamma)$ which is constant along ∂S, we will keep the notation u for its restriction to $L^2(0, L)$.

Let $\alpha = g, l$ denote the gas and liquid phases assumed to be both defined by a mixture of components $i \in \mathcal{C}$ among which the water component denoted by e which can vaporize in the gas phase, and a set of gaseous components $j \in \mathcal{C} \setminus \{e\}$ which can dissolve in the liquid phase. For the sake of simplicity, the model is assumed to be isothermal with a fixed temperature T_e. Following [4], the gas liquid Darcy flow formulation uses the gas pressure p^g, the liquid pressure p^l, and the component fugacities $f = (f_i)_{i\in\mathcal{C}}$ as primary unknowns, denoted by $\mathbf{u} = (p^g, p^l, f)$ in the following. In this formulation, following [16], the component molar fractions $c^\alpha = (c_i^\alpha)_{i\in\mathcal{C}}$ of each phase $\alpha = g, l$ are the functions $c_i^\alpha(\mathbf{u})$ of $\mathbf{u}$ defined by inversion of the equations $f_i^\alpha(c^\alpha, p^g, p^l) = f_i$, $i \in \mathcal{C}$, where f_i^α is the fugacity of the component i in the phase α. In addition, for $\alpha = g, l$, the phase pressure p^α is extended in the absence of the phase in such a way that the closure law $\sum_{i\in\mathcal{C}} c_i^\alpha(\mathbf{u}) = 1$ is always imposed. The phase molar and mass densities, as well as the phase viscosities are denoted in the following by respectively $\zeta^\alpha(p^\alpha, c^\alpha)$, $\rho^\alpha(p^\alpha, c^\alpha)$, $\mu^\alpha(p^\alpha, c^\alpha)$ for $\alpha = g, l$. For the sake of simplicity, for $\xi = \zeta^\alpha$, ρ^α, or μ^α, we will still use the notation $\xi(\mathbf{u})$ for the function $\xi(p^\alpha, c^\alpha(\mathbf{u}))$.
Finally, we define the liquid saturation s^l as the function $s^l(\mathbf{x}, p^l - p^g)$ of $-p_c = p^l - p^g$ defined by the inverse of the monotone graph extension of the opposite of the capillary pressure function $-p_c(\mathbf{x}, .)$, and we set $s^g(\mathbf{x}, .) = 1 - s^l(\mathbf{x}, .)$.

This leads to the following set of equations for the unknowns $\mathbf{u}$ in the porous medium:

$$\begin{cases} \phi\partial_t \sum_{\alpha=g,l} \zeta^\alpha(\mathbf{u}) s^\alpha(\mathbf{x}, p^l - p^g) c_i^\alpha(\mathbf{u}) + \mathrm{div}\Big(\sum_{\alpha=g,l} \zeta^\alpha(\mathbf{u}) c_i^\alpha(\mathbf{u}) \mathbf{V}^\alpha \Big) = 0,\ i \in \mathcal{C},\ \text{on } \Omega \times (0,T), \\ \sum_{i\in\mathcal{C}} c_i^\alpha(\mathbf{u}) = 1,\ \alpha = g, l,\ \text{on } \Omega \times (0,T), \end{cases} \tag{1}$$

coupled with the two phase Darcy laws

$$\mathbf{V}^\alpha = -\frac{k_r^\alpha(\mathbf{x}, s^\alpha(\mathbf{x}, p^l - p^g))}{\mu^\alpha(\mathbf{u})} \mathbf{K}(\mathbf{x}) \Big(\nabla p^\alpha - \rho^\alpha(\mathbf{u}) \mathbf{g} \Big),\ \alpha = g, l,\ \text{on } \Omega \times (0,T), \tag{2}$$

where the function $k_r^\alpha(\mathbf{x}, s^\alpha)$ of the phase saturation s^α is the relative permeability of the phase $\alpha = g, l$, $\mathbf{g}$ is the gravity vector, $\phi(\mathbf{x})$ is the porosity of the porous medium and $\mathbf{K}(\mathbf{x})$ its permeability tensor. The Dirichlet boundary conditions on Γ_D are denoted by $\mathbf{u}_{ext}(\mathbf{x})$ and the initial conditions in the porous medium are denoted by $\mathbf{u}_{init}(\mathbf{x})$. They both typically correspond to pure water and imposed liquid pressure. At the boundary Γ_N, a zero flux boundary condition is imposed for all components.

In the gallery, the primary unknowns, depending only on the x coordinate along the gallery and on the time t, are the gas pressure p and the gas molar fractions $c = (c_i, i \in \mathcal{C})$. The constant gas molar fraction assumption in the section of the gallery corresponds to a strong turbulent diffusivity assumption leading to well-mixed conditions. Note that in Subsection 4.3, this model will be improved by the introduction of an additional gas molar fraction at the interface on the gallery side corresponding to the gas molar fraction in the viscous boundary layer. The gas flow model is defined by a No Pressure Wave (NPW) [17] isothermal pipe flow model. To fix ideas a Forchheimer law is used for the pressure drop given by the two parameters $\alpha_g > 0$, $\beta_g > 0$. The mass conservation of each component $i \in \mathcal{C}$ involves the porous media fluxes at the interface Γ integrated over ∂S and summed over both phases $\alpha = g, l$ assuming an instantaneous vaporization of the liquid phase in the gallery. Denoting by $\mathbf{n}$ the unit normal vector at Γ outward to Ω, and by $|S|$ the surface of the section S, we obtain the following set of equations set on $(0, L) \times (0, T)$:

$$\begin{cases} \partial_t \Big(|S| \zeta^g(p, c) c_i \Big) + \partial_x \Big(|S| \zeta^g(p, c) c_i w \Big) \\ \qquad\qquad = \int_{\partial S} \sum_{\alpha=g,l} \zeta^\alpha(\mathbf{u}) c_i^\alpha(\mathbf{u}) \mathbf{V}^\alpha \cdot \mathbf{n}\ ds,\ i \in \mathcal{C},\ \text{on } (0,L) \times (0,T), \\ \sum_{i\in\mathcal{C}} c_i = 1,\ \text{on } (0,L) \times (0,T), \\ (\alpha_g w + \beta_g |w| w) = -\partial_x p,\ \text{on } (0,L) \times (0,T). \end{cases} \tag{3}$$

The boundary conditions are typically defined by the input gas velocity w_{in} and the input gas molar fractions $c_{in} = (c_{i,in},\ i \in \mathcal{C})$ at the left side of the gallery $x = 0$, and by the output gas pressure p_{out} at the right side of the gallery $x = L$. The initial conditions in the gallery are given by $c_{init} = c_{in}$ and $p_{init} = p_{out}$ (see Figure 1).

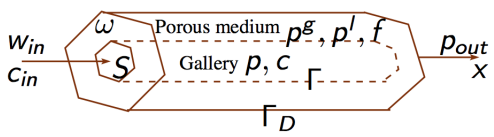

Figure 1: Geometry of the cylindrical domain, and set of unknowns in the porous medium and in the gallery.

At the interface Γ between the gallery and the porous medium the coupling conditions are an adaptation to a 1D configuration for the free flow to those stated in [5]. Compared with [5], the gas pressure jump $p - p^g$ at the interface is neglected since a small flow rate between the porous medium and the gallery is assumed due to the low permeability of the disposal. Hence the coupling conditions account first for the continuity of the gas phase pressure $p^g = p$. Second, as in [5], we impose the continuity of the gas molar fractions $c^g = c$. Third, the thermodynamical equilibrium between the gas phase and the liquid phase at the interface Γ is assumed leading to $f_i = f_i^l = f_i^g = pc_i$ for all $i \in \mathcal{C}$ together with $\sum_{i\in\mathcal{C}} c_i^l(p^g, p^l, f) = 1$ which provides the additional equation for the liquid pressure p^l at the interface. All together, we obtain the following set of coupling conditions at the interface Γ

$$\left\{\begin{array}{rl} p^g &= p, \\ f &= pc, \\ \sum_{i\in\mathcal{C}} c_i^l(p^g, p^l, f) &= 1. \end{array}\right. \tag{4}$$

Let γ denote formally the trace operator on Γ. Using the coupling conditions (4), we can reformulate the model in the gallery (3) as the following set of Ventcel type boundary conditions (see [18]) at the interface Γ for the unknowns $\mathbf{u}$:

$$\left\{\begin{array}{l} \partial_t\Big(|S|\zeta^g(\gamma\mathbf{u})c_i^g(\gamma\mathbf{u})\Big) + \partial_x\Big(|S|\zeta^g(\gamma\mathbf{u})c_i^g(\gamma\mathbf{u})w\Big) \\ \qquad\qquad = \displaystyle\int_{\partial S} \sum_{\alpha=g,l} \zeta^\alpha(\mathbf{u})c_i^\alpha(\mathbf{u})\mathbf{V}^\alpha\cdot\mathbf{n}\, ds,\ i\in\mathcal{C},\ \text{on } \Gamma\times(0,T), \\ \displaystyle\sum_{i\in\mathcal{C}} c_i^\alpha(\gamma\mathbf{u}) = 1,\ \alpha = g, l,\ \text{on } \Gamma\times(0,T), \\ \partial_s\gamma\mathbf{u} = 0,\ \text{on } \Gamma\times(0,T), \end{array}\right. \tag{5}$$

coupled with the closure law

$$(\alpha_g w + \beta_g|w|w) = -\partial_x\gamma p^g,\ \text{on } \Gamma\times(0,T). \tag{6}$$

In summary, the coupled model amounts to find $\mathbf{u}$ on $\Omega\times(0,T)$ satisfying the set of equations (1), the closure laws (2), the boundary conditions (5)-(6) at the interface Γ, together with the boundary conditions for $\mathbf{u}$ on Γ_D and Γ_N, for $\gamma\mathbf{u}$ at $\{x = 0\}$ and at $\{x = L\}$, and the initial conditions at $t = 0$ for $\mathbf{u}$ on Ω, and for $\gamma\mathbf{u}$ on $(0, L)$.

3 Vertex Approximate Gradient (VAG) Discretization

In order to introduce the VAG discretization of our model let us first consider the coupling of a single phase Darcy flow in the porous medium with a 1D single phase Darcy flow in the gallery. The discretization of the VAG fluxes and control volumes will be derived from this simple model and then used for the discretization of the previous full model.

3.1 Linear Model Problem

Let us define γ the trace operator from $H^1(\Omega)$ to $L^2(\Gamma)$, and the function space

$$V = \{u \in H^1(\Omega)\,|\,\gamma u \in H^1(\Gamma), \partial_s\gamma u = 0\}.$$

Keeping the same notation for convenience, the trace operator γ maps V to $H^1(0, L)$. The subspace of V taking into account homogeneous Dirichlet boundary conditions on Γ_D, and at $x = L$ is denoted by

$$V^0 = \{u \in V\,|\,u = 0 \text{ on } \Gamma_D,\ (\gamma u)(L) = 0\}.$$

The space V^0 is endowed with the Hilbertian norm

$$\|u\|_{V^0} = \Big(\int_\Omega |\nabla u(\mathbf{x})|^2 d\mathbf{x} + \int_0^L |\frac{d}{dx}\gamma u(x)|^2 dx\Big)^{\frac{1}{2}}.$$

Let $Q \in L^2(\Omega)$ and $q \in L^2(0,L)$ denote respectively the source terms in the porous medium and in the gallery. Let $\bar{u} \in V$, $w_{in} \in \mathbb{R}$, we consider the following linear model coupling a single phase Darcy flow in the porous medium with a single phase Darcy flow in the gallery:

$$\begin{cases} \mathrm{div}\Big(-\mathbf{K}\nabla u\Big) = Q & \text{on } \Omega, \\ \partial_s \gamma u = 0 & \text{on } \Gamma, \\ \partial_x\Big(-\dfrac{|S|}{\alpha_g}\partial_x \gamma u\Big) = |S|q + \displaystyle\int_{\partial S} -\mathbf{K}\nabla u \cdot \mathbf{n}\, ds & \text{on } (0,L), \\ u = \bar{u} & \text{on } \Gamma_D, \\ -\mathbf{K}\nabla u \cdot \mathbf{n} = 0 & \text{on } \Gamma_N, \\ -\dfrac{1}{\alpha_g}\partial_x \gamma u(0) = w_{in}, & \\ \gamma u(L) = \gamma \bar{u}(L). & \end{cases} \tag{7}$$

Its variational formulation amounts to find $u \in V$ such that $u - \bar{u} \in V^0$ and

$$\int_\Omega \mathbf{K}\nabla u \cdot \nabla v \; d\mathbf{x} + \int_0^L \frac{|S|}{\alpha_g}\partial_x \gamma u \; \partial_x \gamma v \; dx + |S| w_{in} \gamma v(0) = \int_\Omega Q v \; d\mathbf{x} + \int_0^L |S| q \gamma v \; dx. \tag{8}$$

for all $v \in V^0$. The existence and uniqueness of a solution to (8) is readily obtained from the Lax Milgram theorem.

3.2 VAG Discretization of the Linear Model Problem

The VAG discretization [1] is a finite volume discretization of diffusion problem adapted to general meshes and heterogeneous anisotropic media. It is here extended to our model problem coupling the 3D Darcy flow in the porous medium with the 1D Darcy flow in the gallery.

We assume that ω and S are polygonal domains of $\mathbb{R}^2$ and we consider a conforming polyhedral mesh of the domain Ω. It is assumed that the intersection of the mesh with the boundary Γ of the gallery is the tensor product of the 1D mesh of $(0,L)$ defined by $0 = x_0 < x_1 < \cdots < x_{m_x+1} = L$ by the 1D mesh of ∂S defined by the set of distinct points $\mathbf{s}_1, \mathbf{s}_2 \cdots, \mathbf{s}_{m_S}, \mathbf{s}_{m_S+1} = \mathbf{s}_1$ of ∂S in cyclic order.

Let $\mathcal{M}$ denote the set of cells K, $\mathcal{V}$ the set of vertices $\mathbf{s}$, $\mathcal{E}$ the set of edges e, and $\mathcal{F}$ the set of faces σ, of the mesh. We denote by $\mathcal{V}_K$ the set of vertices of each cell $K \in \mathcal{M}$, by $\mathcal{M}_s$ the set of cells sharing the node s, by $\mathcal{V}_\sigma$ the set of nodes and by $\mathcal{E}_\sigma$ the set of edges of the face $\sigma \in \mathcal{F}$. The set of vertices of the mesh belonging to $\{x_m\} \times \partial S$ is denoted by $\mathcal{V}_m$ for all $m = 0, \cdots, m_x + 1$, and we denote by $\mathcal{V}_\Gamma = \bigcup_{m=0,\cdots,m_x+1} \mathcal{V}_m$ the set of nodes of the boundary Γ of the gallery, and by $\mathcal{V}_D = \mathcal{V} \cap \overline{\Gamma}_D$ the set of Dirichlet boundary nodes.

It is assumed that for each face $\sigma \in \mathcal{F}$, there exists a so-called "centre" of the face $\mathbf{x}_\sigma$ such that $\mathbf{x}_\sigma = \sum_{\mathbf{s}\in\mathcal{V}_\sigma} \beta_{\sigma,\mathbf{s}}\, \mathbf{x}_\mathbf{s}$, with $\sum_{\mathbf{s}\in\mathcal{V}_\sigma} \beta_{\sigma,\mathbf{s}} = 1$, where $\beta_{\sigma,\mathbf{s}} \geq 0$ for all $\mathbf{s} \in \mathcal{V}_\sigma$. The face σ is assumed to be star-shaped w.r.t. its centre $\mathbf{x}_\sigma$. Denoting by $\tau_{\sigma,e}$ the triangle joining the face centre $\mathbf{x}_\sigma$ to the edge $e \in \mathcal{E}_\sigma$, it means that the face σ matches with the union for $e \in \mathcal{E}_\sigma$ of the triangles $\tau_{\sigma,e}$.

The previous discretization is denoted by $\mathcal{D}$. Let us define the vector space

$$Y_\mathcal{D} = \{v_K \in \mathbb{R}, v_\mathbf{s} \in \mathbb{R}, K \in \mathcal{M}, \mathbf{s} \in \mathcal{V}\}.$$

The vector space $X_{\mathcal{D}}$ of discrete unknowns is the subspace of $Y_{\mathcal{D}}$ defined by

$$X_{\mathcal{D}} = \{v_{\mathcal{D}} \in Y_{\mathcal{D}} \,|\, v_{\mathbf{s}} = v_{\mathbf{s}'} \text{ for all } \mathbf{s}, \mathbf{s}' \in \mathcal{V}_m, m = 0, \cdots, m_x + 1\}.$$

In the following, for any $v_{\mathcal{D}} \in X_{\mathcal{D}}$ and for all $m = 0, \cdots, m_x + 1$, the notation v_m will stand for the value $v_{\mathbf{s}}$, for all $\mathbf{s} \in \mathcal{V}_m$.

The subspace of $X_{\mathcal{D}}$ with homogeneous Dirichlet boundary conditions on Γ_D and at $x = L$ is defined by

$$X^0_{\mathcal{D}} = \{v_{\mathcal{D}} \in X_{\mathcal{D}} \,|\, v_{\mathbf{s}} = 0 \text{ for all } \mathbf{s} \in \mathcal{V}_D \cup \mathcal{V}_{m_x+1}\}.$$

Following [1], the extension of the VAG discretization to the coupled model is based on conforming Finite Element reconstructions of the gradient operators on Ω and on $(0, L)$, and on non conforming piecewise constant function reconstructions on Ω and on $(0, L)$.

For all $\sigma \in \mathcal{F}$, let us first define the operator $I_\sigma : Y_{\mathcal{D}} \to \mathbb{R}$ such that $I_\sigma(v_{\mathcal{D}}) = \sum_{\mathbf{s} \in \mathcal{V}_\sigma} \beta_{\sigma,\mathbf{s}} v_{\mathbf{s}}$, which is by definition of $\mathbf{x}_\sigma$ a second order interpolation operator at point $\mathbf{x}_\sigma$.

Let us introduce the tetrahedral sub-mesh $\mathcal{T} = \{T_{K,\sigma,e}, e \in \mathcal{E}_\sigma, \sigma \in \mathcal{F}_K, K \in \mathcal{M}\}$ of the mesh $\mathcal{M}$, where $T_{K,\sigma,e}$ is the tetrahedron defined by the cell center $\mathbf{x}_K$ and the triangle $\tau_{\sigma,e}$. For a given $v_{\mathcal{D}} \in Y_{\mathcal{D}}$, we define the function $\Pi_{\mathcal{T}} v_{\mathcal{D}} \in C^0(\overline{\Omega})$ as the continuous piecewise affine function on each tetrahedron T of $\mathcal{T}$ such that $\Pi_{\mathcal{T}} v_{\mathcal{D}}(\mathbf{x}_K) = v_K$, $\Pi_{\mathcal{T}} v_{\mathcal{D}}(\mathbf{s}) = v_{\mathbf{s}}$, and $\Pi_{\mathcal{T}} v_{\mathcal{D}}(\mathbf{x}_\sigma) = I_\sigma(v_{\mathcal{D}})$ for all $K \in \mathcal{M}$, $\mathbf{s} \in \mathcal{V}$, $\sigma \in \mathcal{F}$.

It is easily checked that $\partial_s \gamma \Pi_{\mathcal{T}} v_{\mathcal{D}} = 0$ for all $v_{\mathcal{D}} \in X_{\mathcal{D}}$ which shows that $\Pi_{\mathcal{T}} v_{\mathcal{D}} \in V$ for all $v_{\mathcal{D}} \in X_{\mathcal{D}}$ and we denote by $V_{\mathcal{T}} = \Pi_{\mathcal{T}} X_{\mathcal{D}}$ the finite element subspace of V. Let η_K, and $\eta_{\mathbf{s}}$, $\mathbf{s} \in \mathcal{V}_K$, $K \in \mathcal{M}$ be the finite element nodal functions in $\Pi_{\mathcal{T}} Y_{\mathcal{D}}$ such that $\eta_K(\mathbf{x}_L) = \delta_{K,L}$, $\eta_{\mathbf{s}}(\mathbf{x}_L) = 0$ for all $L \in \mathcal{M}$, and $\eta_K(\mathbf{s}') = 0$, $\eta_{\mathbf{s}}(\mathbf{s}') = \delta_{\mathbf{s},\mathbf{s}'}$ for all $\mathbf{s}' \in \mathcal{V}$. Then, the nodal basis of $V_{\mathcal{T}}$ is defined by η_K, $K \in \mathcal{M}$, $\eta_{\mathbf{s}}$, $\mathbf{s} \in \mathcal{V} \setminus \mathcal{V}_\Gamma$, and $\eta_m = \sum_{\mathbf{s} \in \mathcal{V}_m} \eta_s$, $m = 0, \cdots, m_x + 1$.

Then, we define for all $v_{\mathcal{D}} \in X_{\mathcal{D}}$ the following gradient operators:

$$\nabla_{\mathcal{D}_p} v_{\mathcal{D}} : X_{\mathcal{D}} \to L^2(\Omega)^d \text{ such that } \nabla_{\mathcal{D}_p} v_{\mathcal{D}} = \nabla \Pi_{\mathcal{T}} v_{\mathcal{D}},$$

and

$$\nabla_{\mathcal{D}_g} v_{\mathcal{D}} : X_{\mathcal{D}} \to L^2(0, L) \text{ such that } \nabla_{\mathcal{D}_g} v_{\mathcal{D}} = \partial_x \gamma \Pi_{\mathcal{T}} v_{\mathcal{D}}.$$

One can easily check that

$$\nabla_{\mathcal{D}_g} v_{\mathcal{D}} = \frac{v_{m+1} - v_m}{x_{m+1} - x_m} \text{ on } (x_m, x_{m+1}) \text{ for all } m = 0, \cdots, m_x. \tag{9}$$

In addition to the conforming finite element discretization, the VAG discretization uses two non conforming piecewise constant reconstructions of functions from $X_{\mathcal{D}}$ into respectively $L^2(\Omega)$ and $L^2(0, L)$. The definition of the first operator $\Pi_{\mathcal{D}_p} v_{\mathcal{D}}(\mathbf{x})$ from $X_{\mathcal{D}}$ to $L^2(\Omega)$ is based on the following partition of each cell $K \in \mathcal{M}$

$$K \;=\; \omega_K \bigcup \Big(\bigcup_{\mathbf{s} \in \mathcal{V}_K \setminus (\mathcal{V}_D \cup \mathcal{V}_\Gamma)} \omega_{K,\mathbf{s}} \Big)$$

Then, we set

$$\Pi_{\mathcal{D}_p} v_{\mathcal{D}}(\mathbf{x}) = \begin{cases} v_K & \text{for all } \mathbf{x} \in \omega_K,\ K \in \mathcal{M}, \\ v_{\mathbf{s}} & \text{for all } \mathbf{x} \in \omega_{K,\mathbf{s}},\ \mathbf{s} \in \mathcal{V}_K \setminus (\mathcal{V}_D \cup \mathcal{V}_\Gamma),\ K \in \mathcal{M}. \end{cases} \tag{10}$$

Note that, in the practical case of piecewise constant source terms on the above partition, as it will be the case in the following discretization of the compositional model, the above partition does not

need to be built explicitely. Only the volumes of ω_K and $\omega_{K,s}$ must be prescribed by definition of the coefficients $\alpha_{K,\mathbf{s}} = \frac{|\omega_{K,\mathbf{s}}|}{|K|}$ from which we derive $|\omega_{K,s}| = \alpha_{K,s}|K|$ and $|\omega_K| = (1 - \sum_{s\in\mathcal{V}_K\setminus(\mathcal{V}_D\cup\mathcal{V}_\Gamma)})|K|$ (constrained to be positive) for all $\mathbf{s} \in \mathcal{V}_K \setminus (\mathcal{V}_D \cup \mathcal{V}_\Gamma)$ and $K \in \mathcal{M}$.

For the second reconstruction operator, let us define the points $x_{m+\frac{1}{2}} = \frac{x_m+x_{m+1}}{2}$ for all $m = 0, \cdots, m_x - 1$, $x_{m_x+\frac{1}{2}} = x_{m_x+1} = L$, and $\Delta x_0 = x_{\frac{1}{2}} - x_0$, $\Delta x_m = x_{m+\frac{1}{2}} - x_{m-\frac{1}{2}}$ for all $m = 1, \cdots, m_x$. Then, we set

$$\Pi_{\mathcal{D}_g} v_{\mathcal{D}}(x) = \begin{cases} v_0 & \text{for all } \ x \in (x_0, x_{\frac{1}{2}}), \\ v_m & \text{for all } \ x \in (x_{m-\frac{1}{2}}, x_{m+\frac{1}{2}}),\ m = 1, \cdots, m_x. \end{cases} \tag{11}$$

The VAG discretization of our model problem is obtained by the following non conforming variational formulation: given $\bar{u}_{\mathcal{D}} \in X_{\mathcal{D}}$, find $u_{\mathcal{D}} \in X_{\mathcal{D}}$ such that $u_{\mathcal{D}} - \bar{u}_{\mathcal{D}} \in X^0_{\mathcal{D}}$ and

$$\begin{aligned} \int_\Omega \mathbf{K}\nabla_{\mathcal{D}_p} u_{\mathcal{D}} \cdot \nabla_{\mathcal{D}_p} v_{\mathcal{D}} d\mathbf{x} + \int_0^L \frac{|S|}{\alpha_g} \nabla_{\mathcal{D}_g} u_{\mathcal{D}} \nabla_{\mathcal{D}_g} v_{\mathcal{D}} dx + |S| w_{in} v_0 \\ = \int_\Omega Q \Pi_{\mathcal{D}_p} v_{\mathcal{D}} d\mathbf{x} + \int_0^L |S| q \Pi_{\mathcal{D}_g} v_{\mathcal{D}} dx, \end{aligned} \tag{12}$$

for all $v_{\mathcal{D}} \in X^0_{\mathcal{D}}$.

On the porous medium side, let us define for all $u_{\mathcal{D}} \in X_{\mathcal{D}}$ the VAG fluxes

$$V_{K,\mathbf{s}}(u_{\mathcal{D}}) = \int_K -\mathbf{K}\nabla_{\mathcal{D}_p} u_{\mathcal{D}} \cdot \nabla \eta_{\mathbf{s}} d\mathbf{x} = \sum_{\mathbf{s}'\in\mathcal{V}_K} T_K^{\mathbf{s},\mathbf{s}'}(u_K - u_{\mathbf{s}'}), \tag{13}$$

connecting each cell K to its vertices $\mathbf{s} \in \mathcal{V}_K$ where $T_K^{\mathbf{s},\mathbf{s}'} = -\int_K \mathbf{K}\nabla\eta_{\mathbf{s}} \cdot \nabla\eta_{\mathbf{s}'} d\mathbf{x}$.

On the gallery side, we similarly define for all $u_{\mathcal{D}} \in X_{\mathcal{D}}$ the VAG fluxes

$$V_{m,m+1}(u_{\mathcal{D}}) = \int_{x_m}^{x_{m+1}} -\frac{|S|}{\alpha_g}(\nabla_{\mathcal{D}_g} u_{\mathcal{D}})(\partial_x \eta_{m+1}) dx = T_{m+\frac{1}{2}}(u_m - u_{m+1}), \tag{14}$$

connecting m to $m+1$ for all $m = 0, \cdots, m_x$, where

$$T_{m+\frac{1}{2}} = \int_{x_m}^{x_{m+1}} \frac{|S|}{\alpha_g}(\partial_x \eta_{m+1})^2 dx = \frac{|S|}{(x_{m+1} - x_m)^2} \int_{x_m}^{x_{m+1}} \frac{dx}{\alpha_g}.$$

Let us set $Q_K = \frac{1}{|\omega_K|}\int_{\omega_K} Q(\mathbf{x})d\mathbf{x}$, $Q_{K,\mathbf{s}} = \frac{1}{|\omega_{K,\mathbf{s}}|}\int_{\omega_{K,\mathbf{s}}} Q(\mathbf{x})d\mathbf{x}$ for all $\mathbf{s} \in \mathcal{V}_K \setminus (\mathcal{V}_D \cup \mathcal{V}_\Gamma)$ and $K \in \mathcal{M}$. Then, the variational formulation (12) is equivalent to find $u_{\mathcal{D}} \in X_{\mathcal{D}}$ satisfying the discrete conservation equations in the porous medium

$$\begin{cases} \displaystyle\sum_{\mathbf{s}\in\mathcal{V}_K} V_{K,\mathbf{s}}(u_{\mathcal{D}}) = |K|(1 - \sum_{\mathbf{s}\in\mathcal{V}_K\setminus(\mathcal{V}_D\cup\mathcal{V}_\Gamma)} \alpha_{K,\mathbf{s}})Q_K, & \text{for all } K \in \mathcal{M}, \\ \displaystyle\sum_{K\in\mathcal{M}_{\mathbf{s}}} -V_{K,\mathbf{s}}(u_{\mathcal{D}}) = \sum_{K\in\mathcal{M}_{\mathbf{s}}} |K|\alpha_{K,\mathbf{s}} Q_{K,\mathbf{s}}, & \text{for all } \mathbf{s} \in \mathcal{V} \setminus (\mathcal{V}_D \cup \mathcal{V}_\Gamma), \\ u_{\mathbf{s}} = \bar{u}_{\mathbf{s}}, & \text{for all } \mathbf{s} \in \mathcal{V}_D, \end{cases} \tag{15}$$

coupled with the conservation equations in the gallery

$$\begin{cases} \displaystyle\sum_{\mathbf{s}\in\mathcal{V}_0}\sum_{K\in\mathcal{M}_{\mathbf{s}}} -V_{K,\mathbf{s}}(u_{\mathcal{D}}) + V_{0,1}(u_{\mathcal{D}}) - |S|w_{in} = \int_{x_0}^{x_{1/2}} |S|q dx, \\ \displaystyle\sum_{\mathbf{s}\in\mathcal{V}_m}\sum_{K\in\mathcal{M}_{\mathbf{s}}} -V_{K,\mathbf{s}}(u_{\mathcal{D}}) + V_{m,m+1}(u_{\mathcal{D}}) - V_{m-1,m}(u_{\mathcal{D}}) = \int_{x_{m-1/2}}^{x_{m+1/2}} |S|q dx \quad \text{for all } m = 1, \cdots, m_x, \\ u_{m_x+1} = \bar{u}_{m_x+1}. \end{cases} \tag{16}$$

Note that the right hand side Q does not appear in the conservation equations in the gallery. This is due to our choice of the operator $\Pi_{\mathcal{D}_p}$ which avoids the mixing of the porous medium and the gallery in the control volumes located at nodes $\mathbf{s} \in \mathcal{V}_\Gamma$. This is a crucial property to extend the VAG discretization to the compositional model taking into account the different models and the highly contrasted material properties in the gallery and in the porous medium.

3.3 Extension to the Compositional Model

The VAG scheme has been extended to multiphase Darcy flows in [3] for compositional models. In [2, 4] it is adapted to the case of discontinuous capillary pressures using a phase pressure formulation in order to take into account accurately the saturation jump at the interfaces between different rocktypes. This motivates the choice of the phase pressures as primary unknowns in our model. The current discretization uses ideas of [2, 4] and extends them to the coupling with the 1D free gas flow.

Let us define $\mathbf{u}_\mathcal{D} = (p^g_\mathcal{D}, p^l_\mathcal{D}, f_\mathcal{D}) \in (X_\mathcal{D})^2 \times (X_\mathcal{D})^\mathcal{C}$ as the vector of the discrete unknowns of the coupled model (1)-(2)-(5)-(6). The discretization of the Darcy fluxes for each component $i \in \mathcal{C}$ combines the VAG single phase fluxes, and a phase by phase upwinding of the mobility terms w.r.t. the sign of the flux:

$$V^\alpha_{K,\mathbf{s},i}(\mathbf{u}_\mathcal{D}) = m^\alpha_i(\mathbf{x}_K, \mathbf{u}^{\alpha,up}_{K,\mathbf{s}})\Big(V_{K,\mathbf{s}}(p^\alpha_\mathcal{D}) + g\rho^\alpha_{K,\mathbf{s}} V_{K,\mathbf{s}}(z_\mathcal{D})\Big),$$

with the mobility $m^\alpha_i(\mathbf{x}, \mathbf{u}) = \zeta^\alpha(\mathbf{u}) c^\alpha_i(\mathbf{u}) \frac{k^\alpha_r(\mathbf{x}, s^\alpha(\mathbf{x}, p^l - p^g))}{\mu^\alpha(\mathbf{u})}$, the upwinding

$$\mathbf{u}^{\alpha,up}_{K,\mathbf{s}} = \begin{cases} \mathbf{u}_K & \text{if} \quad V_{K,\mathbf{s}}(p^\alpha_\mathcal{D}) + g\rho^\alpha_{K,\mathbf{s}} V_{K,\mathbf{s}}(z_\mathcal{D}) \geq 0, \\ \mathbf{u}_\mathbf{s} & \text{else}, \end{cases}$$

the averaged density $\rho^\alpha_{K,\mathbf{s}} = \frac{\rho^\alpha(\mathbf{u}_K) + \rho^\alpha(\mathbf{u}_\mathbf{s})}{2}$, and the vector of the vertical coordinates at all d.o.f. $z_\mathcal{D} = \Big(z_K, K \in \mathcal{M}, z_\mathbf{s}, \mathbf{s} \in \mathcal{V}\Big)$.

On the gallery side, the momentum equation $(\alpha_g w + \beta_g |w| w) = -\partial_x p^g$ can be inverted as

$$w = h(\alpha_g, \beta_g, \partial_x p^g) = \frac{\alpha_g - \sqrt{\alpha_g^2 + 4\beta_g |\partial_x p^g|}}{2\beta_g} \frac{\partial_x p^g}{|\partial_x p^g|}.$$

The VAG fluxes in the gallery (14) are extended to this Darcy-Forchheimer law using a one quadrature point formula as follows

$$V_{m,m+1}(p^g_\mathcal{D}) = |S| h\left(\alpha_g(x_{m+\frac{1}{2}}), \beta_g(x_{m+\frac{1}{2}}), \frac{p^g_{m+1} - p^g_m}{x_{m+1} - x_m}\right),$$

and the discretization of the Darcy-Forchheimer fluxes for each component $i \in \mathcal{C}$ is defined by

$$V_{m,m+1,i}(\mathbf{u}_\mathcal{D}) = \zeta^g(\mathbf{u}^{up}_{m,m+1}) c^g_i(\mathbf{u}^{up}_{m,m+1}) V_{m,m+1}(p^g_\mathcal{D}),$$

with the upwinding

$$\mathbf{u}^{up}_{m,m+1} = \begin{cases} \mathbf{u}_m, & \text{if} \quad V_{m,m+1}(p^g_\mathcal{D}) \geq 0, \\ \mathbf{u}_{m+1}, & \text{else}, \end{cases}$$

for all $m = 0, \cdots, m_x$.

For $N \in \mathbb{N}^*$, let us consider the time discretization $t^0 = 0 < t^1 < \cdots < t^{n-1} < t^n \cdots < t^N = T$ of the time interval $[0, T]$. We denote the time steps by $\Delta t^n = t^n - t^{n-1}$ for all $n = 1, \cdots, N$.

The initial conditions are given in the porous medium by $\mathbf{u}_\nu^0 = \mathbf{u}_{init}(\mathbf{x}_\nu)$ for all $\nu \in \mathcal{M} \cup \Big(\mathcal{V} \setminus (\mathcal{V}_D \cup \mathcal{V}_\Gamma)\Big)$. In the gallery, they are defined for all $m = 0, \cdots, m_x$ by $p_m^{g,0} = p_{init}$, $f_m^0 = p_{init} c_{init}$, and $p_m^{l,0}$ obtained from the equation $\sum_{i \in \mathcal{C}} c_i^l(\mathbf{u}_m^0) = 1$.

The system of discrete equations in the porous medium at time step t^n accounts for the discrete molar conservation of each component $i \in \mathcal{C}$ and the sum to one of the molar fractions of each phase in each control volume $K \in \mathcal{M}$ and $\mathbf{s} \in \mathcal{V} \setminus (\mathcal{V}_D \cup \mathcal{V}_\Gamma)$, together with the Dirichlet boundary conditions for $\mathbf{s} \in \mathcal{V}_D$:

$$\left\{\begin{array}{l} (1 - \displaystyle\sum_{\mathbf{s} \in \mathcal{V}_K \setminus (\mathcal{V}_D \cup \mathcal{V}_\Gamma)} \alpha_{K,\mathbf{s}}) \phi_K \frac{n_i(\mathbf{x}_K, \mathbf{u}_K^n) - n_i(\mathbf{x}_K, \mathbf{u}_K^{n-1})}{\Delta t^n} + \displaystyle\sum_{\alpha = g,l} \sum_{\mathbf{s} \in \mathcal{V}_K} V_{K,\mathbf{s},i}^\alpha(\mathbf{u}_\mathcal{D}^n) = 0, \; K \in \mathcal{M}, \\ \displaystyle\sum_{K \in \mathcal{M}_\mathbf{s}} \alpha_{K,\mathbf{s}} \phi_K \frac{n_i(\mathbf{x}_K, \mathbf{u}_\mathbf{s}^n) - n_i(\mathbf{x}_K, \mathbf{u}_\mathbf{s}^{n-1})}{\Delta t^n} - \displaystyle\sum_{\alpha = g,l} \sum_{K \in \mathcal{M}_\mathbf{s}} V_{K,\mathbf{s},i}^\alpha(\mathbf{u}_\mathcal{D}^n) = 0, \; \mathbf{s} \in \mathcal{V} \setminus (\mathcal{V}_D \cup \mathcal{V}_\Gamma), \\ \displaystyle\sum_{i \in \mathcal{C}} c_i^\alpha(\mathbf{u}_\nu^n) = 1, \; \nu \in \mathcal{M} \cup \Big(\mathcal{V} \setminus (\mathcal{V}_D \cup \mathcal{V}_\Gamma)\Big), \; \alpha = g, l, \\ \mathbf{u}_\mathbf{s}^n = \mathbf{u}_{ext}(\mathbf{x}_\mathbf{s}), \; \mathbf{s} \in \mathcal{V}_D, \end{array}\right.$$

with $\phi_K = \int_K \phi(\mathbf{x}) d\mathbf{x}$, and the number of moles per unit matrix volume of the components $i \in \mathcal{C}$

$$n_i(\mathbf{x}, \mathbf{u}) = \sum_{\alpha = g,l} \zeta^\alpha(\mathbf{u}) s^\alpha(\mathbf{x}, p^l - p^g) c_i^\alpha(\mathbf{u}).$$

This system is coupled to the following equations in the gallery at time step t^n accounting for the discrete molar conservation of each component $i \in \mathcal{C}$, the sum to one of the molar fractions, and the Dirichlet conditions at the right side of the gallery:

$$\left\{\begin{array}{l} \dfrac{\Delta x_0}{\Delta t^n} |S| \left(\zeta^g(\mathbf{u}_0^n) c_i^g(\mathbf{u}_0^n) - \zeta^g(\mathbf{u}_0^{n-1}) c_i^g(\mathbf{u}_0^{n-1})\right) + V_{0,1,i}(\mathbf{u}_\mathcal{D}^n) - |S| \zeta^g(\mathbf{u}_0^n) c_{i,in} w_{in} \\ \qquad\qquad = \displaystyle\sum_{\mathbf{s} \in \mathcal{V}_0} \sum_{\alpha = g,l} \sum_{K \in \mathcal{M}_\mathbf{s}} V_{K,s,i}^\alpha(\mathbf{u}_\mathcal{D}^n), \\ \dfrac{\Delta x_m}{\Delta t^n} |S| \left(\zeta^g(\mathbf{u}_m^n) c_i^g(\mathbf{u}_m^n) - \zeta^g(\mathbf{u}_m^{n-1}) c_i^g(\mathbf{u}_m^{n-1})\right) + V_{m,m+1,i}(\mathbf{u}_\mathcal{D}^n) - V_{m-1,m,i}(\mathbf{u}_\mathcal{D}^n) \\ \qquad\qquad = \displaystyle\sum_{\mathbf{s} \in \mathcal{V}_m} \sum_{\alpha = g,l} \sum_{K \in \mathcal{M}_\mathbf{s}} V_{K,\mathbf{s},i}^\alpha(\mathbf{u}_\mathcal{D}^n), \; m = 1, \cdots, m_x, \\ \displaystyle\sum_{i \in \mathcal{C}} c_i^l(\mathbf{u}_m^n) = 1, \; m = 0, \cdots, m_x + 1, \\ \displaystyle\sum_{i \in \mathcal{C}} c_i^g(\mathbf{u}_m^n) = 1, \; m = 0, \cdots, m_x, \\ c^g(\mathbf{u}_{m_x+1}^n) = c^g(\mathbf{u}_{m_x}^n), \quad p_{m_x+1}^{g,n} = p_{out}. \end{array}\right.$$

4 Numerical experiments

To assess the coupled model and its discretisation, let us consider in this section three test cases all sharing the following setting.

Let ω and S be the disks of center 0 and radius respectively $r_\omega = 10$ m and $r_S = 2$ m. We consider a polyhedral radial mesh of size $n_x \times n_\theta \times n_r$ of the domain $\Omega = (0, L) \times (\omega \setminus \overline{S})$, $L = 1000$ m. The mesh is exponentially refined in the radial direction at the interface of the gallery Γ to account for the steep gradient of the capillary pressure at the porous medium gallery interface (see Figure 2). In

addition to the water component e, we consider the air gaseous component denoted by a with the Henry constant $H_a = 6\ 10^9$ Pa at the fixed temperature $T_e = 300$ K. The gas molar density is given by $\zeta^g(p^g) = \frac{p^g}{RT_e}$ mol.m^{-3}, and the liquid molar density is fixed to $\zeta^l = 55555$ mol.m^{-3}. The phase viscosities are fixed to $\mu^g = 18.51\ 10^{-6}$ Pa.s^{-1} and $\mu^l = 10^{-3}$ Pa.s^{-1}. The mass densities are defined by $\rho^\alpha = \zeta^\alpha \sum_{i\in\mathcal{C}} c_i^\alpha M_i$ with the molar masses of the components $M_a = 29\ 10^{-3}$ Kg, $M_e = 18\ 10^{-3}$ Kg. The fugacities of the components in the gas phase are given by Dalton's law for an ideal mixture of perfect gas $f_i^g = c_i^g p^g$, $i = e, a$. The fugacities of the components in the liquid phase are given by Henry's law for the dissolution of the air component in the liquid phase $f_a^l = c_a^l H_a(T_e)$, and by Raoult-Kelvin's law for the water component in the liquid phase $f_e^l = c_e^l P_{sat}(T_e)\exp\Big(\frac{-(p^g-p^l)}{\zeta^l(p^l)RT_e}\Big)$, where $P_{sat}(T_e)$ is the vapour pressure of the pure water. The solution of the equation $f^\alpha(c^\alpha, p^g, p^l) = f$ leads to the following component molar fractions c^α as functions of $\mathbf{u}$:

$$\begin{cases} c_e^l(\mathbf{u}) = \dfrac{f_e}{P_{sat}(T_e)}\exp\Big(\dfrac{(p^g-p^l)}{\zeta^l(p^l)RT_e}\Big), & c_a^l(\mathbf{u}) = \dfrac{f_a}{H_a(T_e)}, \\ c_e^g(\mathbf{u}) = \dfrac{f_e}{p^g}, & c_a^g(\mathbf{u}) = \dfrac{f_a}{p^g}. \end{cases} \tag{17}$$

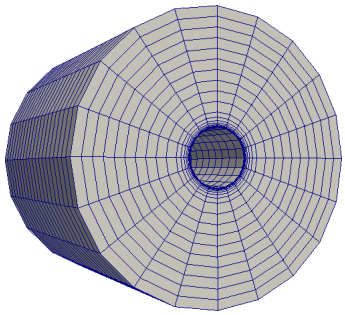

Figure 2: Radial mesh $n_x \times n_\theta \times n_r$ of the domain Ω with $n_r = n_\theta = n_x = 20$ refined at the interface Γ in the radial direction. The figure is zoomed by a factor 50 in the (y, z) directions.

The porous medium is initially saturated by the liquid phase with imposed pressure $p_{init}^l = 40\ 10^5$ Pa and composition $c_{a,init}^l = 0$, $c_{e,init}^l = 1$. At the external boundary $r = r_\omega$ the water pressure is fixed to $p_{ext}^l = p_{init}^l$, with an input composition $c_{a,ext}^l = 0$, $c_{e,ext}^l = 1$. On both sides $x = 0$ and $x = L$ of the porous medium, zero flux boundary conditions are imposed for all components. The initial condition in the gallery is given by $p_{init} = 10^5$ Pa and $c_{e,init}$ is defined by the relative humidity

$$H_{r,init} = \frac{c_{e,init} p_{init}}{P_{sat}(T_e)} = 0.5.$$

We consider an input gas velocity w_{in} depending on time (see Figures 4, 9), a fixed input water molar fraction $c_{e,in} = c_{e,init}$ at the left side $x = 0$ of the gallery, and a fixed output pressure $p_{out} = p_{init}$ at the right side $x = L$ of the gallery (see Figure 3). The relative permeabilities and capillary pressure in the porous medium are given by the following Van-Genuchten laws

$$k_r^l(s^l) = \begin{cases} 0 & \text{if} \quad s^l < s_r^l, \\ 1 & \text{if} \quad s^l > 1 - s_r^g, \\ \sqrt{\bar{s}^l}\Big(1 - (1 - (\bar{s}^l)^{1/m})^m\Big)^2 & \text{if} \quad s_r^l \le s^l \le 1 - s_r^g, \end{cases}$$

$$k_r^g(s^g) = \begin{cases} 0 & \text{if} \quad s^g < s_r^g, \\ 1 & \text{if} \quad s^g > 1 - s_r^l, \\ \sqrt{1 - \bar{s}^l}\Big(1 - (\bar{s}^l)^{1/m}\Big)^{2m} & \text{if} \quad s_r^g \le s^g \le 1 - s_r^l, \end{cases}$$

and

$$s^l(-p_c) = s_r^l + (1 - s_r^l - s_r^g)\frac{1}{\left(1 + (\frac{p_c}{P_r})^n\right)^m},$$

with

$$\bar{s}^l = \frac{s^l - s_r^l}{1 - s_r^l - s_r^g}.$$

The Darcy Forchheimer parameters defining the pressure drop in the gallery are set to $\alpha_g = 0$ and $\beta_g = 10^{-3}$ Kg.m^{-4}.

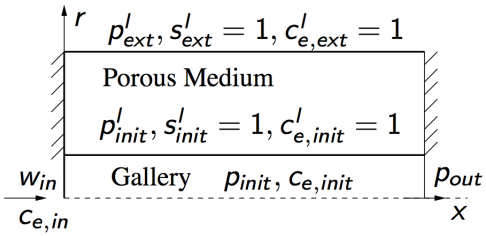

Figure 3: (x, r) cut of the disposal and initial and boundary conditions of the test case.

4.1 Comparison with a quasi analytical stationary solution

In this first test case, we consider a single rocktype in the porous medium defined by the parameters $n = 1.49$, $s_r^l = 0.4$, $s_r^g = 0$, $P_r = 15\ 10^6$ Pa of the Van-Genuchten laws accounting for the Callovo-Oxfordian argillites (COx). The permeability is assumed isotropic with $\mathbf{K} = 5\ 10^{-20}$ m^2 the porosity is set to $\phi = 0.15$.

The input velocity w_{in} is fixed to 1 m.s^{-1} during the first 4000 days, 0.01 m.s^{-1} during the next 4000 days, and 0 m.s^{-1} during the remaining simulation (see Figure 4). The simulation is run over a period of 10000 days with an initial time step of 100 seconds and a maximum time step of 50 days. The time step is also refined down to 0.1 day in the neighbouhood of $t = 4000$ days and $t = 8000$ days. The time stepping is fixed for all meshes and chosen fine enough in order to provide a time discretization error smaller than the space discretization error.

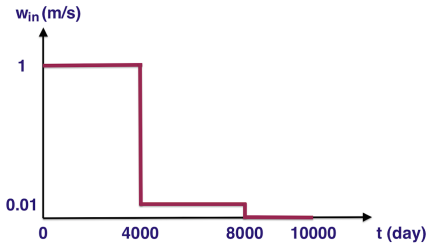

Figure 4: Input velocity w_{in} as a function of time.

4.1.1 Approximate Stationary Solution

In order to validate the simulation, an approximate stationary solution is computed for each value of the input gas velocity w_{in}. In this approximate model, the vaporization of the water component is kept but the dissolution of air is neglected. The gravity is also set to zero since the gravity forces are

small compared with the capillary and pressure gradient forces. The pressure drop along the gallery can also be neglected meaning that the pressure in the gallery is equal to p_{init}. Last but not least, it is observed in the porous medium that the longitudinal derivatives are small compared with the radial derivatives due to the strong gradient of the capillary pressure at the porous medium gallery interface. Hence they will be neglected in our approximate model. Thanks to these assumptions, the stationary solution can be reduced to a single ordinary differential equation (ODE) for the water molar fraction in the gas phase along the gallery $c_e(x)$.

From the above assumptions, the approximate stationary solution $\mathbf{u}(x,r)$ depends only on x and r and satisfies the following simplified system in the porous medium

$$\left\{\begin{array}{l} \frac{\partial}{\partial r}\left(\frac{\zeta^g k_r^g}{\mu^g}\mathbf{K}r\frac{\partial}{\partial r}p^g\right)+\frac{\partial}{\partial r}\left(\frac{\zeta^l k_r^l}{\mu^l}\mathbf{K}r\frac{\partial}{\partial r}p^l\right)=0,\\ \frac{\partial}{\partial r}\left(\frac{c_a^g\zeta^g k_r^g}{\mu^g}\mathbf{K}r\frac{\partial}{\partial r}p^g\right)=0. \end{array}\right. \tag{18}$$

From the coupling conditions, at the porous medium gallery interface $r = r_S$, the gas pressure is fixed to $p^g(x,r_S) = p(x) = p_{init}$ and $c_e^g(x,r_S) = c_e(x)$. From the thermodynamical equilibrium of the water component at the interface, we can compute the capillary pressure at the interface as a function of $c_e(x)$ by the following formula:

$$p_c(c_e(x)) = -\zeta^l RT_e \ln\left(\frac{c_e(x)p_{init}}{P_{sat}(T_e)}\right)$$

Let us define $V_a = \frac{c_a^g\zeta^g k_r^g}{\mu^g}\mathbf{K}r\frac{\partial}{\partial r}p^g$ and the total velocity $V_T = \sum_{\alpha=l,g}\frac{\zeta^\alpha k_r^\alpha}{\mu^\alpha}\mathbf{K}r\frac{\partial}{\partial r}p^\alpha$. We can deduce by integration of (18) taking into account the boundary conditions $p^g(x,r_S) = p_{init}$, $c_e^g(x,r_S) = c_e(x)$, $c_a^g(x,r_S) = 1 - c_e(x)$, $p_c(x,r_S) = p_c(c_e(x))$, $p^l(x,r_\omega) = p_{ext}^l$, $c_e^l(x,r_\omega) = 1$, $c_a^l(x,r_\omega) = 0$, that $V_a = 0$ and that V_T depends only on x and is given by the following function of $c_e(x)$:

$$V_T(c_e(x)) = \frac{\zeta^l\mathbf{K}}{\mu^l\log(\frac{r_\omega}{r_S})}\left(p_{ext}^l - p_{init} + \int_0^{p_c(c_e(x))} k_r^l(s^l(-u))du\right).$$

Turning to the equations in the gallery, $c_e(x)$ and $w(x)$ are solutions of the following system of ODEs

$$\left\{\begin{array}{rl} \frac{d}{dx}\Big(\zeta^g(p_{init})w(x)c_e(x)\Big) &= \frac{2}{r_S^2}V_T(c_e(x)), x\in(0,L),\\ \frac{d}{dx}\Big(\zeta^g(p_{init})w(x)(1-c_e(x))\Big) &= 0, x\in(0,L),\\ c_e(0) &= c_{e,in},\\ w(0) &= w_{in}. \end{array}\right.$$

The second equation yields $w(x) = w_{in}\frac{(1-c_{e,in})}{1-c_e(x)}$, $\forall x\in(0,L)$ and the above system reduces to the following ODE for $c_e(x)$:

$$\left\{\begin{array}{rl} \zeta^g(p_{init})w_{in}(1-c_{e,in})\frac{d}{dx}\left(\frac{c_e(x)}{1-c_e(x)}\right) &= \frac{2}{r_S^2}V_T(c_e(x)), \quad x\in(0,L),\\ c_e(0) &= c_{e,in}, \end{array}\right. \tag{19}$$

which is numerically integrated.

4.1.2 Numerical results

The numerical solution obtained with the mesh $80\times50\times80$ is exhibited in Figures 5, 6 and 7. Figure 5 plots the average relative humidity in the gallery defined by $H_r(t) = \frac{1}{L}\int_0^L\frac{c_e(x,t)p(x,t)}{P_{sat}(T_e)}dx$ as a function

of time. It also compares the numerical stationary relative humidities obtained as a function of x for each value of w_{in} with the ones obtained with the approximate stationary analytical model (19). A very good match can be checked in Figure 5 for the three input velocities. Figure 6 plots as a function of time the gas volume in the porous medium and the volumetric flow rates at the porous medium gallery interface for both phases. Figure 7 plots the stationary numerical liquid saturation at the porous medium gallery interface (represented in the gallery) and in the porous medium for each value of w_{in}. At the opening of the gallery at $t = 0$, we observe in Figures 5 an increase of the average relative humidity $H_r(t)$ up to almost 0.95 in a few seconds due to a large liquid flow rate (see Figure 6) at the interface. Then, the flow rate decreases and we observe a drying of the gallery due to the ventilation at $w_{in} = 1$ m.s^{-1} down to an average relative humidity slightly above $H_{r,init}$ in a few days. Meanwhile the gas penetrates slowly into the porous medium reaching a stationary state with around 167 m^3 of gas in say 4000 days (see Figure 6). When the input velocity is reduced to 0.01 m.s^{-1}, we observe first a rapid increase of $H_r(t)$ in say 100 days due to the reduced ventilation followed by a convergence to a second stationary state with $H_r(t) = 0.74$ in the gallery and around 137 m^3 of gas in the porous medium. Note in Figure 6 that the gas flow rate is entering in the porous medium between say 4600 and 7000 days although the volume of gas in the porous medium is still decreasing. This is due to a larger mass of air dissolved in the liquid phase entering into the gallery than the mass of air entering into the porous medium in the gas phase. At equilibrium, at time say between 7000 and 8000 days, the mass of air entering into the gallery dissolved in the liquid phase is compensated by the mass of air entering into the porous media in the gas phase. When w_{in} is set to 0 m.s^{-1}, $H_r(t)$ reaches a value above 1 corresponding to a negative capillary pressure and $s^l = 1$ at the interface and the gas disappears from the porous medium in around 1400 days. The value above 1 of the relative humidity is due to the fact that the model does not take into account the appearance of the liquid phase in the gallery side.

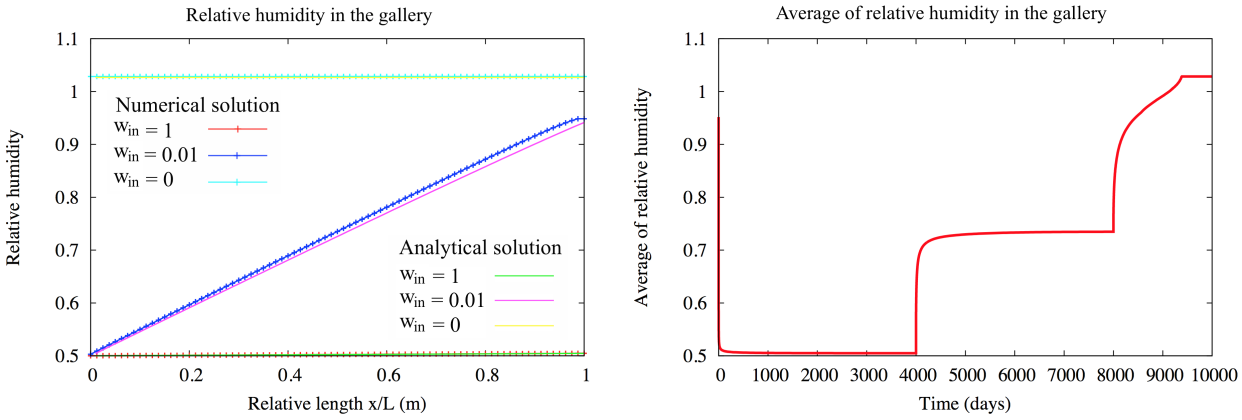

Figure 5: Stationary relative humidity in the gallery for each value of w_{in} compared with its approximate "analytical" solution (left); average of the relative humidity in the gallery as a function of time (right).

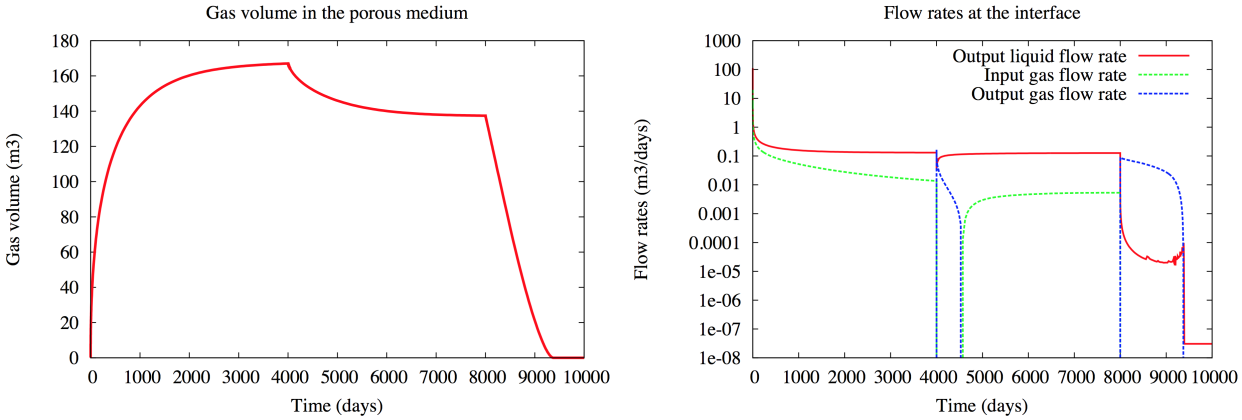

Figure 6: Gas Volume in the porous medium as a function of time (left); input and output flow rates at the interface Γ for the gas and liquid phases (right) as a function of time (an input flow rate enters into the porous medium).

(a) $w_{in} = 1$ m.s^{-1} (b) $w_{in} = 0.01$ m.s^{-1}

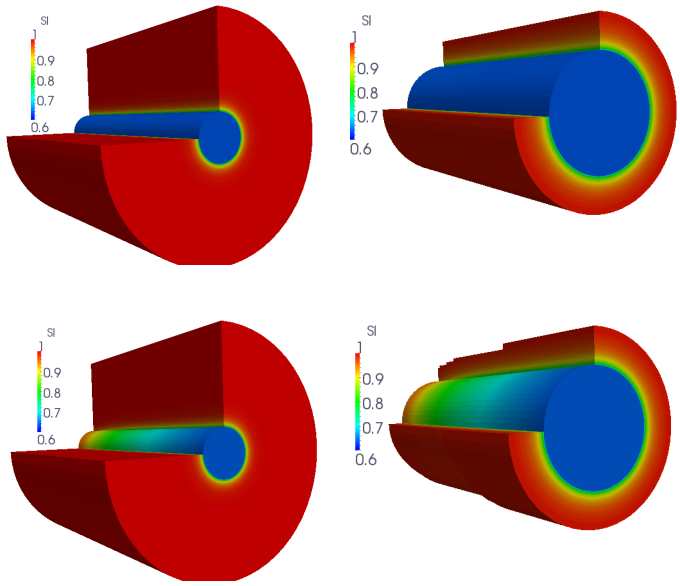

Figure 7: Stationary liquid saturation s^l obtained for $w_{in} = 1$ m.s^{-1} (a) and for $w_{in} = 0.01$ m.s^{-1} (b). The bottom figures zoom the liquid saturation in the porous medium below the threshold value 0.99. In the gallery the liquid saturation corresponds to the saturation at the interface function of x.

Figure 8 exhibits the convergence of the volume of gas in the porous medium as a function of time and of $H_r(t)$ for the five different meshes $20 \times 20 \times 20$, $40 \times 40 \times 40$, $60 \times 50 \times 60$, $70 \times 50 \times 70$ and $80 \times 50 \times 80$. Table 1 shows the numerical behaviour of the simulations for these five meshes. A rather good scalability of the linear and nonlinear solvers and of the CPU time w.r.t. the mesh size is obtained. The linear system is solved using the GMRES iterative solver preconditioned by ILU0, and the linear and nonlinear stopping criteria are fixed to respectively 10^{-6} and 10^{-5} for the relative residuals.

mesh	$N_{\Delta t}$	N_{Chop}	N_{Newton}	N_{GMRes}	CPU(s)
$20 \times 20 \times 20$	615	0	3.12	11.5	890
$30 \times 30 \times 30$	615	0	3.12	15	3250
$40 \times 40 \times 40$	615	0	3.12	19	8050
$60 \times 50 \times 60$	615	0	3.15	24.5	17300
$70 \times 50 \times 70$	640	6	3.27	57	105200
$80 \times 50 \times 80$	666	10	3.35	77	135300

Table 1: For each mesh : number $N_{\Delta t}$ of successful time steps, number N_{Chop} of time step chops, number N_{Newton} of Newton iterations per successful time step, number N_{GMRes} of GMRes iterations by Newton iteration, CPU time in seconds.

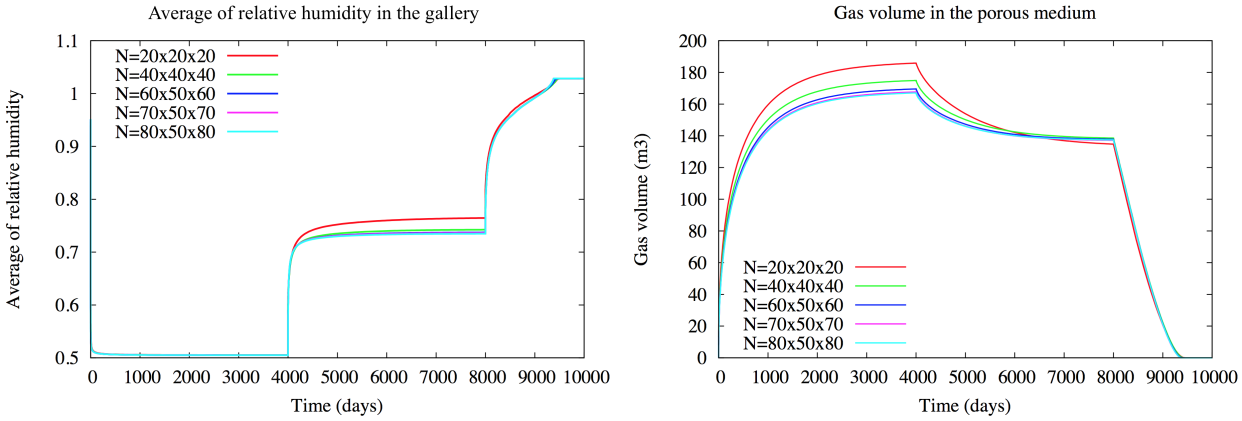

Figure 8: Average relative humidity in the gallery $H_r(t)$ (left) and gas volume in the porous medium as a function of time (right) for the five meshes.

4.2 Heterogeneous anisotropic test case

This second test case considers two different rocktypes in the porous medium. For $r_S < r < r_I = 3$ m we consider a damaged rock with isotropic permeability $\mathbf{K} = 5\ 10^{-18}$ m^2 and a porosity $\phi = 0.15$, and for $r > r_I$ we consider the Callovo-Oxfordian argillites (COx) with the same porosity $\phi = 0.15$ and the anisotropic permeability defined by $\mathbf{K} = \begin{pmatrix} \lambda & 0 & 0 \\ 0 & \lambda & 0 \\ 0 & 0 & \frac{\lambda}{10} \end{pmatrix}$ with $\lambda = 5\ 10^{-20}$ m^2 in the x, y, z Cartesian coordinates where z is the vertical coordinate and x the direction of the Gallery. The Van-Genuchten parameters are defined by $n = 1.50$, $s_r^l = 0.2$, $s_r^g = 0$, $P_r = 5\ 10^6$ Pa in the damaged zone, and by $n = 1.49$, $s_r^l = 0.4$, $s_r^g = 0$, $P_r = 15\ 10^6$ Pa in the COx region.

The input velocity w_{in} is fixed to 1 m.s^{-1} during the first 3000 days, to 0.1 m.s^{-1} during the next 3000 days, and to 0.01 m.s^{-1} during the remaining simulation (see Figure 9). The simulation is run over a period of 20000 days with an initial time step of 100 seconds and a maximum time step of 1000 days. The time step is also refined down to 0.1 day in the neighbouhood of $t = 3000$ days and $t = 6000$ days. This time stepping is fixed for all meshes and chosen fine enough in order to provide a time discretization error smaller than the space discretization error on all meshes. All the other parameters of the data set are the same as in the previous test case.

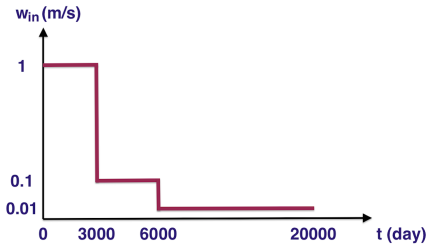

Figure 9: Input velocity w_{in} as a function of time.

As in the previous test case, the Figures 10, 11, and 12 exhibit the numerical solution obtained with the mesh $60 \times 60 \times 60$. Figure 10 plots the relative humidity in the gallery at the end of the simulation as a function of x, as well as the average relative humidity $H_r(t)$. Figure 11 shows the gas volume in the porous medium as a function of time, and the volumetric flow rates for both phases at the porous medium gallery interface as a function of time. Figure 12 plots the liquid saturation at the end of the simulation. Compared with the previous test case, a larger volume of gas enters into the porous medium due to the larger permeability of the damaged zone. The effect of the anisotropy along the vertical direction in the COx region is also clear in the right liquid saturation plot in Figure 12.

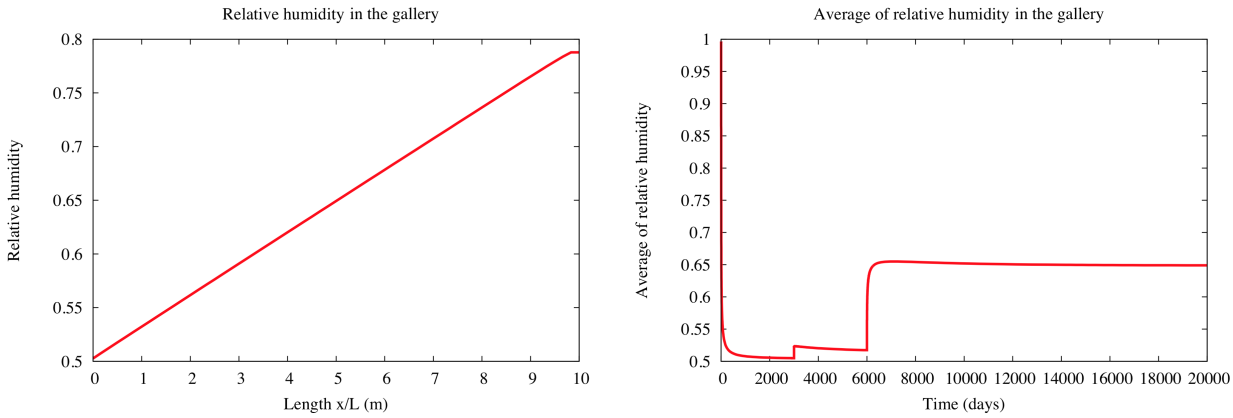

Figure 10: Relative humidity in the gallery at the end of the simulation (left); average of the relative humidity in the gallery as a function of time (right).

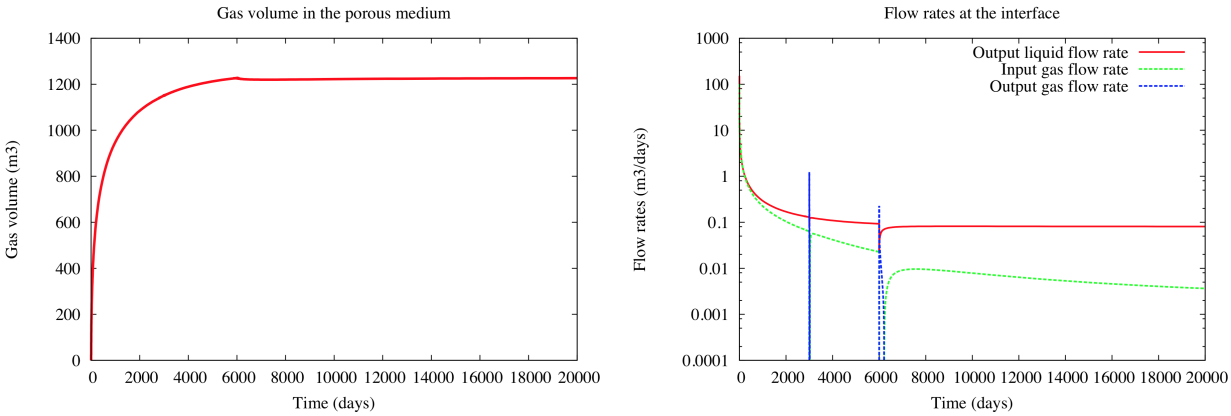

Figure 11: Gas Volume in the porous medium as a function of time (left); input and output flow rates at the interface Γ for the gas and liquid phases (right) as a function of time (an input flow rate enters into the porous medium).

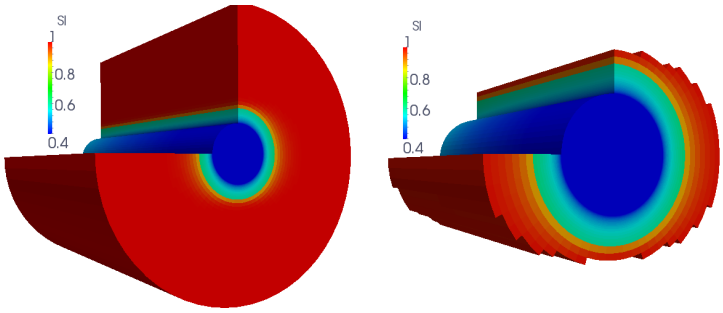

Figure 12: Liquid saturation s^l at the end of the simulation. At the right, the liquid saturation in the porous medium is plotted only below the threshold value 0.99. In the gallery the liquid saturation corresponds to the saturation at the interface function of x.

Figure 13 exhibits the convergence of the volume of gas in the porous medium as a function of time and of $H_r(t)$ for the five different meshes $30 \times 30 \times 30$, $40 \times 40 \times 40$, $50 \times 50 \times 50$, $60 \times 60 \times 60$ and $70 \times 70 \times 70$. Table 2 shows the numerical behaviour of the simulations for these five meshes with again a rather good scalability of the linear and nonlinear solvers and of the CPU time w.r.t. the mesh size.

mesh	$N_{\Delta t}$	N_{Chop}	N_{Newton}	N_{GMRes}	CPU(s)
$30 \times 30 \times 30$	409	0	3.31	15	2200
$40 \times 40 \times 40$	409	0	3.34	18	6800
$50 \times 50 \times 50$	409	0	3.37	20	14050
$60 \times 60 \times 60$	409	0	3.40	23	20100
$70 \times 70 \times 70$	409	0	3.45	25	34700

Table 2: For each mesh : number $N_{\Delta t}$ of successful time steps, number N_{Chop} of time step chops, number N_{Newton} of Newton iterations per successful time step, number N_{GMRes} of GMRes iterations by Newton iteration, CPU time in seconds.

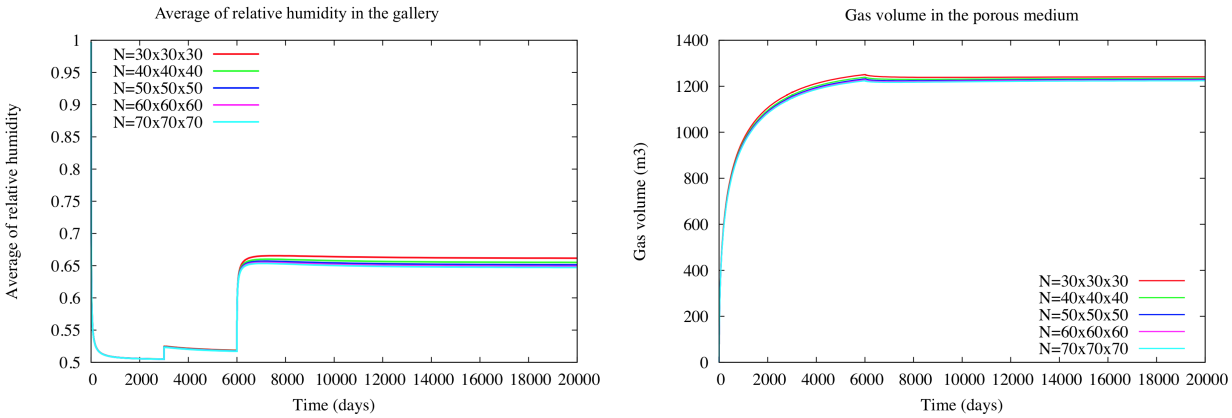

Figure 13: Average in space of the relative humidity in the gallery (left) and gas volume in the porous medium (right) as a function of time.

4.3 Model with gas molar fraction and diffusion at the interface

The previous model can be improved by the introduction of two gas molar fractions in the gallery instead of a single one. The first one corresponds to the gas molar fraction in the viscous boundary layer at the interface Γ on the gallery side. By the assumption of continuity of the gas molar fraction, it is equal to $c^g(\gamma \mathbf{u})$. Outside of this boundary layer, the second gas molar fraction is assumed to be constant in the section of the gallery thanks to a strong turbulent mixing. This second gas molar fraction is denoted by c which is now an additional independent unknown. Another additional unknown is the normal gas velocity at the interface on the gallery side denoted by v_n with the normal oriented outward of the porous medium (see Figure 14).

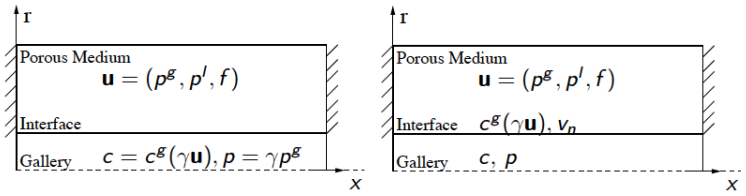

Figure 14: Main unknowns in the porous medium, at the interface and in the gallery for the previous model (left) and the new model (right).

The new system is looking for $\mathbf{u}$, v_n, p and c satisfying the porous medium system (1)-(2), coupled with the following modified system at the interface Γ

$$\left\{\begin{array}{l} \displaystyle\sum_{\alpha=g,l} \zeta^\alpha(\mathbf{u}) c_i^\alpha(\mathbf{u}) \mathbf{V}^\alpha \cdot \mathbf{n} = \\ \qquad\qquad \zeta^g(\gamma\mathbf{u})\Big(c_i^g(\gamma\mathbf{u})(v_n)^+ + c_i(v_n)^- + \frac{D^g}{\delta}(c_i^g(\gamma\mathbf{u}) - c_i)\Big),\ i \in \mathcal{C},\ \text{on } \Gamma \times (0,T), \\ \displaystyle\sum_{i\in\mathcal{C}} c_i^\alpha(\gamma\mathbf{u}) = 1,\ \alpha = g, l,\ \text{on } \Gamma \times (0,T), \\ \gamma p^g = p - \rho^g(p,c) g(z - \frac{1}{|S|}\int_S dz),\ \text{on } \Gamma \times (0,T), \end{array}\right. \tag{20}$$

and the conservation equations along the gallery

$$\left\{\begin{array}{l} \partial_t\Big(|S|\zeta^g(\gamma p^g,c)c_i\Big)+\partial_x\Big(|S|\zeta^g(\gamma p^g,c)c_i w\Big) \\ \qquad\qquad = \displaystyle\int_{\partial S}\sum_{\alpha=g,l}\zeta^\alpha(\mathbf{u})c_i^\alpha(\mathbf{u})\mathbf{V}^\alpha\cdot\mathbf{n}\;ds,\; i\in\mathcal{C},\;\text{ on }(0,L)\times(0,T), \\ \displaystyle\sum_{i\in\mathcal{C}}c_i=1,\;\text{ on }(0,L)\times(0,T), \end{array}\right. \tag{21}$$

with $(\alpha_g w+\beta_g|w|w)=-\partial_x\gamma p^g$. Note that it results from the first and second equations in (20) and from the second equation in (21) that

$$v_n=\frac{1}{\zeta^g(\gamma\mathbf{u})}\sum_{\alpha=g,l}\zeta^\alpha(\mathbf{u})\mathbf{V}^\alpha\cdot\mathbf{n}.$$

In (20), we have used the notation $a^+=\max(a,0)$ and $a^-=\min(a,0)$. The interface conditions (20) account for the gas pressure continuity, the thermodynamical equilibrium, and the molar flux continuity. The gas pressure γp^g at the interface assumes an hydrostatic pressure in the section S. In most cases, this hydrostatic correction can actually be neglected.

Following [5], the molar flux continuity takes into account the two point diffusion flux $\frac{D^g}{\delta}(c_i^g(\gamma\mathbf{u})-c_i)$ between the gas molar fraction at the interface $c^g(\gamma\mathbf{u})$ and the mean gas molar fraction c in the gallery, where D^g is the Fickian diffusion coefficient set to $D^g=2\ 10^{-5}$ m^2.s^{-1} in the following tests. This diffusion term is dominant compared with the convective term for the water component, and it is clearly essential to allow the component molar fluxes $\int_{\partial S}\sum_{\alpha=g,l}\zeta^\alpha(\mathbf{u})c_i^\alpha(\mathbf{u})\mathbf{V}^\alpha\cdot\mathbf{n}\;ds$ at the interface to take different signs (typically positive for the water component and negative for the air component).

The parameter δ is a convection diffusion boundary layer thickness at the interface Γ for the water component molar fraction in the gallery. It depends on the velocity and on the turbulent diffusion in the gallery. In practice, the parameter δ can be obtained as a function of $\mathbf{x}$ on Γ using a diagonal approximation of the Steklov Poincaré operator related to the stationary convection diffusion equation in the gallery. Let us refer to [19] for details and for a numerical comparison of our reduced model with a full dimensional model which exhibits a very good match for the relative humidity in the gallery and for the liquid and gas flow rates at the interface. Note also that the previous model is recovered at the limit when δ goes to zero implying that $\gamma c^g(\gamma\mathbf{u})=c$.

In the following tests, the influence of the parameter δ on the solution of the previous test case is investigated for $\delta=10^{-1},10^{-2},10^{-3},10^{-4},10^{-5}$ m. It is compared with the previous model solution corresponding to $\delta\to 0^+$. All the physical and numerical parameters are the same than in the previous test case including the input velocity w_{in} (see Figure 9). The initial time step is changed to $\Delta t=0.1$ s and the mesh size is fixed to $40\times 40\times 40$. It is clear from the numerical results exhibited in Figures 15, 16 and 17 that the larger δ, the higher the average relative humidity at the interface, the lower the output liquid flux at the interface, and the lower the average relative humidity in the gallery. The convergence of the solution to the solution of the previous model when $\delta\to 0^+$ is also checked.

The difference between both models is also seen to be much larger at small times when the liquid flux at the interface is high due to the instantaneous opening of the gallery. At larger times, once the liquid flux at the interface has sufficiently decreased (the threshold value depending on δ) both models roughly match. Away from a very short transient solution, we can classically observe in Figures 16 and 17 the two stages of the drying process. The first stage corresponds to a roughly constant drying rate and liquid influx at the interface. This first stage lasts until the porous medium

at the interface is not sufficiently desaturated to slow down the liquid flow rate at the interface. The second stage corresponds to a decreasing liquid flow rate at the interface together with an increasing gas saturation in the porous medium until they reach a stationary state roughly described by the analytical solution of subsection 4.1. Table 3 exhibits the good numerical behavior of the Newton solver for a large range of δ.

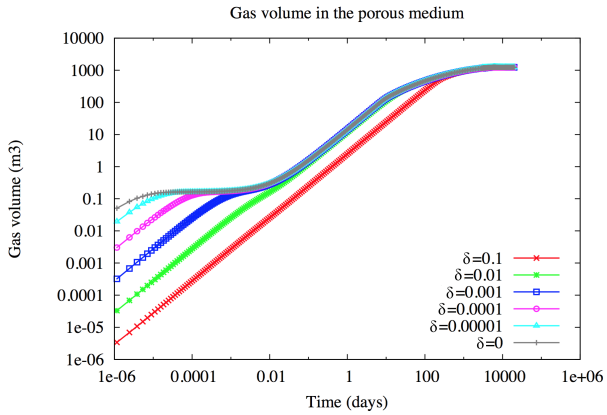

Figure 15: Gas volume in the porous medium as a function of time.

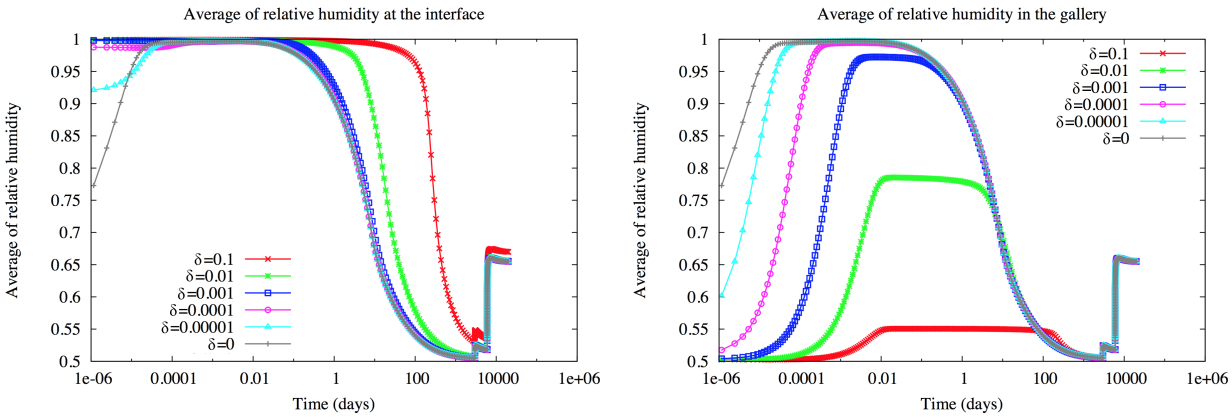

Figure 16: Average in space of the relative humidity at the interface (left) and in the gallery (right) as a function of time.

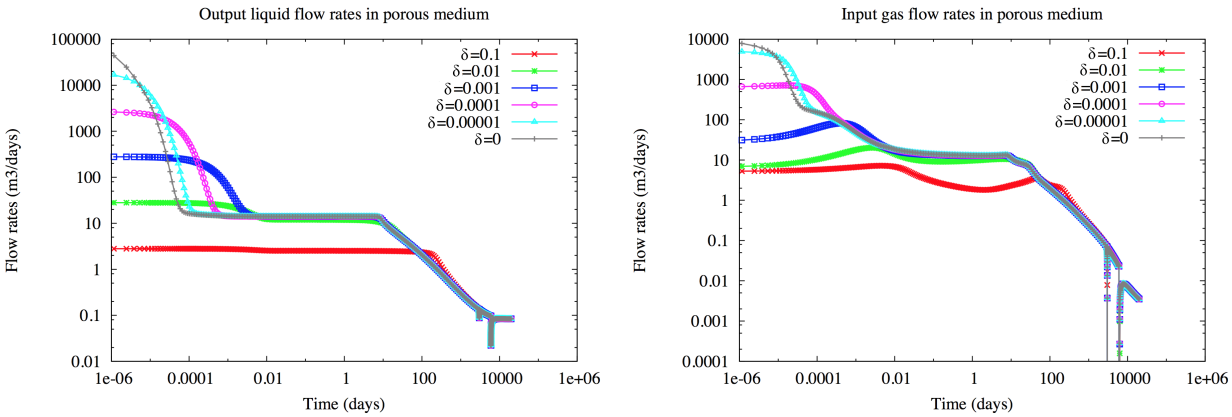

Figure 17: Output liquid flow rates (left) and input gas flow rates (right) in the porous medium as a function of time.

δ	$N_{\Delta t}$	N_{Chop}	N_{Newton}	N_{GMRes}	CPU(s)
10^{-1}	464	0	3.26	11.9	7064
10^{-2}	464	0	3.36	14.6	5971
10^{-3}	464	0	3.43	15.6	7631
10^{-4}	464	0	3.55	16.5	6353
10^{-5}	464	0	3.67	18.1	6630
0	464	0	3.71	19.7	6863

Table 3: For the mesh $40 \times 40 \times 40$ and each value of δ : number $N_{\Delta t}$ of successful time steps, number N_{Chop} of time step chops, number N_{Newton} of Newton iterations per successful time step, number N_{GMRes} of GMRes iterations by Newton iteration, CPU time in seconds.

5 Convergence analysis of a simplified model

We consider the following simplified model using the Richards approximation in the porous medium and a single component equation in the gallery with linear pressure drop

$$\left\{\begin{array}{l} \phi\partial_t(\zeta^l\mathcal{S}^l(.,u)) + \mathrm{div}(\zeta^l\mathbf{V}^l) = Q, \\ \partial_t(|S|\zeta^g(p)) + \partial_x(-\dfrac{1}{\alpha_g}|S|\widetilde{\zeta^g}(p)\partial_x p) = \displaystyle\int_{\partial S}\zeta^l\mathbf{V}^l\cdot\mathbf{n}\;ds + |S|q, \\ \mathbf{V}^l = -\dfrac{k_r^\alpha(.,\mathcal{S}^l(.,u))}{\mu^l}\mathbf{K}\Big(\nabla u - M^l\zeta^l\mathbf{g}\Big), \quad p = g(\gamma(u)). \end{array}\right. \tag{22}$$

The only primary unknown in the porous medium is the liquid pressure denoted by u. The liquid mass density is assumed to be fixed to $M^l\zeta^l$ where M^l is the molar mass of the liquid phase and ζ^l is considered constant. The thermodynamical equilibrium at the interface Γ is accounted for by the relation $p = g(\gamma(u))$ with $g \in C^1(\mathbb{R},\mathbb{R}^+)$, $0 < g'(q) \leq c_2$ for all $q \in \mathbb{R}$ and for a given constant $c_2 > 0$. The function g is a regularization for large positive u of $p = \frac{P_{sat}(T)}{c_e}e^{\frac{u}{\zeta^l RT_e}}$ for given constants $1 \geq c_e > 0$ and $T_e > 0$. The molar gas density is set to $\zeta^g(p) = \frac{p}{RT_e}$ and is truncated in the flux term such that $\widetilde{\zeta^g}(p)$ is assumed to be a non decreasing function in $C^1(\mathbb{R}^+,\mathbb{R}^+)$ bounded from below and above by two strictly positive constants and with a bounded derivative.

To simplify the convergence analysis, we consider in this section Dirichlet boundary conditions at the boundary $\partial\Omega \setminus \overline{\Gamma}$ of Ω still denoted by Γ_D, and at both ends $x = 0$ and $x = L$ of $(0, L)$. Let us define the function space

$$U = \{u \in H^1(\Omega) \,|\, \partial_s\gamma u = 0\},$$

and its subspace $U^0 = U \cap H^1_{\Gamma_D}(\Omega)$ with zero trace on Γ_D.

Let $\mathcal{C}(\Omega\times[0,T))$ be the subspace of functions φ of $C^\infty\Big(\overline{\Omega}\times[0,T]\Big)$ vanishing in a neighbourhood of $t = T$, $\overline{\Gamma}_D$ and $\partial\omega \times \{0, L\}$, and such that $\partial_s\varphi = 0$ in a neighbourhood of $\overline{\Gamma}$. Given $\bar{u} \in V$, $u_{init,p} \in L^2(\Omega)$, and $u_{init,g} \in L^2(0, L)$ the variational formulation of the simplified coupled model amounts to find $u \in L^2\Big(0,T;U\Big)$ with $u - \bar{u} \in L^2\Big(0,T;U^0\Big)$ and $g(\gamma u) - g(\gamma\bar{u}) \in L^2\Big(0,T;H^1_0(\Gamma)\Big)$

such that for all $\varphi \in \mathcal{C}(\Omega \times [0,T))$ one has

$$\left\{\begin{array}{l} -\displaystyle\int_0^T \int_\Omega \phi(\mathbf{x})\zeta^l s^l(\mathbf{x},u(\mathbf{x},t))\partial_t\varphi(\mathbf{x},t)d\mathbf{x}dt - \int_\Omega \phi\zeta^l s^l(\mathbf{x},u_{init,p}(\mathbf{x}))\varphi(\mathbf{x},0)d\mathbf{x} \\ -\displaystyle\int_0^T \int_0^L |S|\zeta^g(g(\gamma u)(x,t))\partial_t\gamma\varphi(x,t)dxdt - \int_0^L |S|\zeta^g(g(u_{init,g})(x))\gamma\varphi(x,0)dx \\ +\displaystyle\int_0^T \int_\Omega \zeta^l \frac{k_r^l(\mathbf{x},s^l(u(\mathbf{x},t)))}{\mu^l}\mathbf{K}(\nabla u(\mathbf{x},t) - M^l\zeta^l\mathbf{g})\cdot\nabla\varphi(\mathbf{x},t)d\mathbf{x}dt \\ +\displaystyle\int_0^T \int_0^L \frac{1}{\alpha_g(x)}|S|\widetilde{\zeta^g}(g(\gamma u)(x,t))\partial_x g(\gamma u)(x,t)\partial_x\gamma\varphi(x,t)dxdt \\ =\displaystyle\int_0^T \Big(\int_\Omega Q(\mathbf{x},t)\varphi(\mathbf{x},t)d\mathbf{x} + \int_0^L |S|q(x,t)\gamma\varphi(x,t)dx\Big)dt. \end{array}\right. \tag{23}$$

We make the following additional *assumptions on the data*:

- It is assumed that $k_r^l(\mathbf{x},s)$ is a measurable function w.r.t. $\mathbf{x}$ and continuous w.r.t. s, and such that $0 < k_{min} \le k_r^l(\mathbf{x},s) \le k_{max}$ for all $(\mathbf{x},s) \in \Omega \times [0,1]$.
- $s^l(\mathbf{x},u) \in [0,1]$ for all $(\mathbf{x},u) \in \Omega\times\mathbb{R}$ with $s^l(\mathbf{x},u) = s_j^l(u)$ for a.e. $\mathbf{x} \in \Omega_j$ and all $u \in \mathbb{R}$, where s_j^l is a non decreasing Lipschitz continuous function with constant L_s and $(\Omega_j)_{j\in J}$ is a finite family of disjoint connected polyhedral open sets such that $\bigcup_{j\in J}\overline{\Omega_j} = \overline{\Omega}$.
- It is assumed that there exists a constant L_{sp} such that $|s^l(x,v) - s^l(x,u)| \le L_{sp}|g(v) - g(u)|$ for all $\mathbf{x} \in \Omega$ and $(u,v) \in \mathbb{R}^2$.
- The permeability tensor $\mathbf{K}$ is a measurable function on the space of symmetric 3 dimensional matrices such that there exist $0 < \underline{\lambda} \le \overline{\lambda}$ with $\underline{\lambda}|\xi|^2 \le (\mathbf{K}(\mathbf{x})\xi,\xi) \le \overline{\lambda}|\xi|^2$ for all $\mathbf{x} \in \overline{\Omega}$.
- $\alpha_g \in L^\infty(0,L)$ is such that $0 < \underline{\alpha}_g \le \alpha_g(x) \le \overline{\alpha}_g$ for all $x \in (0,L)$.
- The porosity ϕ belongs to $L^\infty(\Omega)$ with $0 < \underline{\phi} \le \phi(\mathbf{x}) \le \overline{\phi}$ for all $\mathbf{x} \in \Omega$.
- It is assumed that $Q \in L^2(\Omega\times(0,T))$ and $q \in L^2((0,L)\times(0,T))$.

Remark 5.1 *The VAG discretization and convergence analysis detailed below for the model* (22) *can be readily adapted to another simplified model coupling the Richards equation in the porous medium to a 1D convection diffusion equation for the water molar fraction c_e at given constant velocity w, constant diffusion coefficient $D^g > 0$, and at given constant pressure p.*

$$\left\{\begin{array}{l} \phi\partial_t(\zeta^l\mathcal{S}^l(.,u)) + \mathrm{div}(\zeta^l\mathbf{V}^l) = Q, \\ \partial_t(|S|\zeta^g(p)c_e) + \partial_x\Big(|S|\zeta^g(p)(wc_e - D^g\partial_x c_e)\Big) = \displaystyle\int_{\partial S}\zeta^l\mathbf{V}^l\cdot\mathbf{n}\,ds + |S|q, \\ \mathbf{V}^l = -\dfrac{k_r^\alpha(.,\mathcal{S}^l(.,u))}{\mu^l}\mathbf{K}\Big(\nabla u - M^l\zeta^l\mathbf{g}\Big), \quad c_e = \bar{g}(\gamma(u)), \end{array}\right. \tag{24}$$

As for (22)*, the thermodynamical equilibrium at the interface Γ is accounted for by the relation $c_e = \bar{g}(\gamma(u))$ with $\bar{g} \in C^1(\mathbb{R},\mathbb{R}^+)$, $0 < \bar{g}'(q) \le c_2$ for all $q \in \mathbb{R}$ and for a given constant $c_2 > 0$. Here the function $\bar{g}$ is a regularization for large positive u of $c_e = \frac{p_{sat}(T_e)}{p}e^{\frac{u}{\zeta^l RT_e}}$ for given constants $p > 0$ and $T_e > 0$.*

The model (24) *is a rather good approximation of the full model thanks to the weak liquid inflow from the porous medium to the gallery and to the small pressure drop in the gallery.*

5.1 Vertex Approximate Gradient Discretization

Taking into account the new boundary conditions, the subspace $X_{\mathcal{D}}^0$ of $X_{\mathcal{D}}$ becomes

$$X_{\mathcal{D}}^0 = \{v_{\mathcal{D}} \in X_{\mathcal{D}} \,|\, v_{\mathbf{s}} = 0 \text{ for all } \mathbf{s} \in \mathcal{V}_D \cup \mathcal{V}_0 \cup \mathcal{V}_{m_x+1}\},$$

with $\mathcal{V}_{\mathcal{D}} = \mathcal{V} \cap \Gamma_D$. The reconstruction operator $\Pi_{\mathcal{D}_p}$ is still defined by (10) with this new definition of $\mathcal{V}_D$. The definition of the reconstruction operator $\Pi_{\mathcal{D}_g}$ taking into account the new boundary condition at $x = 0$ is given by

$$\Pi_{\mathcal{D}_g} v_{\mathcal{D}}(x) = v_m \text{ for all } x \in (x_{m-\frac{1}{2}}, x_{m+\frac{1}{2}}),\ m = 1, \cdots, m_x.$$

with $x_{\frac{1}{2}}$ changed to 0 compared with section 3. Other definitions are unchanged compared with section 3.

For $v \in X_{\mathcal{D}}$, and a function $k \in C^0(\mathbb{R}, \mathbb{R})$, we define $k(v) \in X_{\mathcal{D}}$ as follows: $k(v)_{\mathbf{s}} = k(v_{\mathbf{s}})$ for all $\mathbf{s} \in \mathcal{V}$ and $k(v)_K = k(v_K)$ for all $K \in \mathcal{M}$. Then, given $u_{\mathcal{D}}^0 \in X_{\mathcal{D}}$ and $\bar{u}_{\mathcal{D}} \in X_{\mathcal{D}}$, the discretization of the coupled model (23) looks for $u_{\mathcal{D}}^n \in X_{\mathcal{D}}$ with $u_{\mathcal{D}}^n - \bar{u}_{\mathcal{D}} \in X_{\mathcal{D}}^0$ for all $n = 1, \cdots, N$ such that for all $v_{\mathcal{D}} \in X_{\mathcal{D}}^0$

$$\left\{\begin{array}{l}
\displaystyle\int_\Omega \phi(\mathbf{x})\zeta^l \frac{s^l(\mathbf{x}, \Pi_{\mathcal{D}_p} u_{\mathcal{D}}^n(\mathbf{x})) - s^l(\mathbf{x}, \Pi_{\mathcal{D}_p} u_{\mathcal{D}}^{n-1}(\mathbf{x}))}{\Delta t^n} \Pi_{\mathcal{D}_p} v_{\mathcal{D}}(\mathbf{x}) d\mathbf{x} \\
\displaystyle + \int_0^L |S| \frac{\zeta^g(\Pi_{\mathcal{D}_g} g(u_{\mathcal{D}}^n)(x)) - \zeta^g(\Pi_{\mathcal{D}_g} g(u_{\mathcal{D}}^{n-1})(x))}{\Delta t^n} \Pi_{\mathcal{D}_g} v_{\mathcal{D}}(x) dx \\
\displaystyle + \int_\Omega \zeta^l \frac{k_r^l(\mathbf{x}, s^l(\mathbf{x}, \Pi_{\mathcal{D}_p} u_{\mathcal{D}}^n(\mathbf{x})))}{\mu^l} \mathbf{K}(\nabla_{\mathcal{D}_p} u_{\mathcal{D}}^n(\mathbf{x}) - M^l \zeta^l \mathbf{g}) \cdot \nabla_{\mathcal{D}_p} v_{\mathcal{D}}(\mathbf{x}) d\mathbf{x} \\
\displaystyle + \int_0^L \frac{1}{\alpha_g(x)} |S| \widetilde{\zeta^g}(\Pi_{\mathcal{D}_g} g(u_{\mathcal{D}}^n)(x)) \nabla_{\mathcal{D}_g} g(u_{\mathcal{D}}^n)(x) \nabla_{\mathcal{D}_g} v_{\mathcal{D}}(x) dx \\
\displaystyle = \frac{1}{\Delta t^n} \int_{t^{n-1}}^{t^n} \Big(\int_\Omega Q(\mathbf{x}, t) \Pi_{\mathcal{D}_p} v_{\mathcal{D}}(\mathbf{x}) d\mathbf{x} + \int_0^L |S| q(x, t) \Pi_{\mathcal{D}_g} v_{\mathcal{D}}(x) dx \Big) dt.
\end{array}\right. \tag{25}$$

5.2 Convergence analysis

Let ρ_T denote the insphere diameter of a given tetrahedron $T \in \mathcal{T}$, h_T its diameter, and $h_{\mathcal{T}} = \max_{T \in \mathcal{T}} h_T$. We will assume in the convergence analysis that the family of tetrahedral submeshes $\mathcal{T}$ is shape regular in the sense that $\theta_{\mathcal{T}} = \max_{T \in \mathcal{T}} \frac{h_T}{\rho_T}$ will be bounded for the family of meshes. The following Lemmas are simple adaptations of the Lemmas already obtained in [7].

Lemma 5.1 *There exist $C_1, C_2 > 0$ depending only on $\theta_{\mathcal{T}}$ such that for all $u \in X_{\mathcal{D}}$*

$$\|\Pi_{\mathcal{D}_p} u\|_{L^2(\Omega)} \le C_1 \|\Pi_{\mathcal{T}} u\|_{L^2(\Omega)} \quad \text{and} \quad \|\Pi_{\mathcal{D}_g} u\|_{L^2(0,L)} \le C_2 \|\gamma \Pi_{\mathcal{T}} u\|_{L^2(0,L)}. \tag{26}$$

We deduce from Lemma 5.1, the following discrete Poincaré inequalities.

Lemma 5.2 *There exist $C_5, C_6 > 0$ depending only on $\theta_{\mathcal{T}}$ such that for all $u \in X_{\mathcal{D}}^0$*

$$\|\Pi_{\mathcal{D}_p} u\|_{L^2(\Omega)} \le C_5 \|\nabla_{\mathcal{D}_p} u\|_{L^2(\Omega)^3} \quad \text{and} \quad \|\Pi_{\mathcal{D}_g} u\|_{L^2(0,L)} \le C_6 \|\nabla_{\mathcal{D}_g} u\|_{L^2(0,L)}. \tag{27}$$

Lemma 5.3 *There exists $C_3 > 0$ depending only on $\theta_{\mathcal{T}}$ such that, for all $u \in X_{\mathcal{D}}$,*

$$\|\Pi_{\mathcal{D}_p} u - \Pi_{\mathcal{T}} u\|_{L^2(\Omega)} + \|\Pi_{\mathcal{D}_g} u - \gamma \Pi_{\mathcal{T}} u\|_{L^2(0,L)} \le C_3\ h_{\mathcal{T}} \|\Pi_{\mathcal{T}} u\|_V. \tag{28}$$

Lemma 5.3 imply in particular that there exists $C > 0$ depending only on $\theta_{\mathcal{T}}$ such that

$$\|\Pi_{\mathcal{D}_p}\bar{u}_{\mathcal{D}} - \bar{u}\|_{L^2(\Omega)} + \|\Pi_{\mathcal{D}_g}\bar{u}_{\mathcal{D}} - \bar{u}\|_{L^2(0,L)} \leq C\Big((1+h_{\mathcal{T}})\|\Pi_{\mathcal{T}}\bar{u}_{\mathcal{D}} - \bar{u}\|_V + h_{\mathcal{T}}\|\bar{u}\|_V\Big).$$

Next, for any smooth function $\varphi \in C^\infty(\overline{\Omega})$ such that $\partial_s\varphi = 0$ on Γ, let us define the projection $P_{\mathcal{D}}\varphi$ on $X_{\mathcal{D}}$ by $(P_{\mathcal{D}}\varphi)_K = \varphi(\mathbf{x}_K), K \in \mathcal{M}$, $(P_{\mathcal{D}}\varphi)_{\mathbf{s}} = \varphi(\mathbf{x}_{\mathbf{s}}), \mathbf{s} \in \mathcal{V}$. We have the following classical finite element approximation result.

Lemma 5.4 *For all $\varphi \in C^\infty(\overline{\Omega})$ such that $\partial_s\varphi = 0$ on Γ, there exists $C(\varphi) > 0$ depending only on φ and $\theta_{\mathcal{T}}$ such that*

$$\|\varphi - \Pi_{\mathcal{T}}P_{\mathcal{D}}\varphi\|_V \leq C(\varphi)h_{\mathcal{T}}.$$

Let us set $X_{\mathcal{D},\Delta t} = (X_{\mathcal{D}})^N$, and for all $v_{\mathcal{D}} = (v_{\mathcal{D}}^n)_{n=1,\cdots,N} \in X_{\mathcal{D},\Delta t}$ let us define for all $n = 1, \cdots, N$

$$\begin{aligned}
&\Pi_{\mathcal{D}_p,\Delta t}v_{\mathcal{D}}(\mathbf{x},t) = \Pi_{\mathcal{D}_p}v_{\mathcal{D}}^n(\mathbf{x}) \text{ for all } (\mathbf{x},t) \in \Omega \times (t^{n-1},t^n],\\
&\Pi_{\mathcal{D}_g,\Delta t}v_{\mathcal{D}}(x,t) = \Pi_{\mathcal{D}_g}v_{\mathcal{D}}^n(x) \text{ for all } (x,t) \in (0,L) \times (t^{n-1},t^n],\\
&\Pi_{\mathcal{T},\Delta t}v_{\mathcal{D}}(\mathbf{x},t) = \Pi_{\mathcal{T}}v_{\mathcal{D}}^n(\mathbf{x}) \text{ for all } (\mathbf{x},t) \in \Omega \times (t^{n-1},t^n],\\
&\nabla_{\mathcal{D}_p,\Delta t}v_{\mathcal{D}}(\mathbf{x},t) = \nabla_{\mathcal{D}_p}v_{\mathcal{D}}^n(\mathbf{x}) \text{ for all } (\mathbf{x},t) \in \Omega \times (t^{n-1},t^n],\\
&\nabla_{\mathcal{D}_g,\Delta t}v_{\mathcal{D}}(x,t) = \nabla_{\mathcal{D}_g}v_{\mathcal{D}}^n(x) \text{ for all } (x,t) \in (0,L) \times (t^{n-1},t^n].
\end{aligned}$$

Let $u_{\mathcal{D}} = (u_{\mathcal{D}}^n)_{n=1,\cdots,N}$, the given solution to (25), we also define the functions $s^l_{\mathcal{D}_p,\Delta t}(\mathbf{x},t) = s^l(\mathbf{x}, \Pi_{\mathcal{D}_p,\Delta t}u_{\mathcal{D}}(\mathbf{x},t))$, $p_{\mathcal{D}_g,\Delta t}(x,t) = g(\Pi_{\mathcal{D}_g,\Delta t}u_{\mathcal{D}}(x,t))$, and

$$\begin{aligned}
&\delta_{\mathcal{D}}s^l_{\mathcal{D}_p,\Delta t}(\mathbf{x},t) = \frac{s^l(\mathbf{x},\Pi_{\mathcal{D}_p}u_{\mathcal{D}}^n(\mathbf{x})) - s^l(\mathbf{x},\Pi_{\mathcal{D}_p}u_{\mathcal{D}}^{n-1}(\mathbf{x}))}{\Delta t^n} \text{ for all } (\mathbf{x},t) \in \Omega \times (t^{n-1},t^n],\\
&\delta_{\mathcal{D}}p_{\mathcal{D}_g,\Delta t}(x,t) = \frac{\Pi_{\mathcal{D}_g}g(u_{\mathcal{D}}^n)(x) - \Pi_{\mathcal{D}_g}g(u_{\mathcal{D}}^{n-1})(x)}{\Delta t^n} \text{ for all } (x,t) \in (0,L) \times (t^{n-1},t^n].
\end{aligned}$$

Let us set for all $v_{\mathcal{D}} \in X_{\mathcal{D}}^0$

$$\begin{aligned}
A^n_{\mathcal{D}_p}(v_{\mathcal{D}}) &= \int_\Omega \phi(\mathbf{x})\zeta^l \frac{s^l(\mathbf{x},\Pi_{\mathcal{D}_p}u_{\mathcal{D}}^n(\mathbf{x})) - s^l(\mathbf{x},\Pi_{\mathcal{D}_p}u_{\mathcal{D}}^{n-1}(\mathbf{x}))}{\Delta t^n}\Pi_{\mathcal{D}_p}v_{\mathcal{D}}(\mathbf{x})d\mathbf{x}\\
&= \frac{1}{\Delta t^n}\int_{t^{n-1}}^{t^n}\int_\Omega \phi(\mathbf{x})\zeta^l\delta_{\mathcal{D}}s^l_{\mathcal{D}_p,\Delta t}(\mathbf{x},t)\Pi_{\mathcal{D}_p}v_{\mathcal{D}}(\mathbf{x})d\mathbf{x}dt,
\end{aligned} \tag{29}$$

$$\begin{aligned}
A^n_{\mathcal{D}_g}(v_{\mathcal{D}}) &= \int_0^L \frac{|S|}{RT_e}\frac{\Pi_{\mathcal{D}_g}g(u_{\mathcal{D}}^n)(x) - \Pi_{\mathcal{D}_g}g(u_{\mathcal{D}}^{n-1})(x)}{\Delta t^n}\Pi_{\mathcal{D}_g}v_{\mathcal{D}}(x)dx\\
&= \frac{1}{\Delta t^n}\int_{t^{n-1}}^{t^n}\int_0^L \frac{|S|}{RT_e}\delta_{\mathcal{D}}p_{\mathcal{D}_g,\Delta t}(x,t)\Pi_{\mathcal{D}_g}v_{\mathcal{D}}(x)dxdt,
\end{aligned} \tag{30}$$

$$\begin{aligned}
B^n_{\mathcal{D}_p}(v_{\mathcal{D}}) &= \int_\Omega \zeta^l \frac{k_r^l(\mathbf{x},s^l(\mathbf{x},\Pi_{\mathcal{D}_p}u_{\mathcal{D}}^n(\mathbf{x})))}{\mu^l}\mathbf{K}\Big(\nabla_{\mathcal{D}_p}u_{\mathcal{D}}^n(\mathbf{x}) - M^l\zeta^l\mathbf{g}\Big)\cdot\nabla_{\mathcal{D}_p}v_{\mathcal{D}}(\mathbf{x})d\mathbf{x}\\
&= \frac{1}{\Delta t^n}\int_{t^{n-1}}^{t^n}\int_\Omega \zeta^l\frac{k_r^l(\mathbf{x},s^l_{\mathcal{D}_p,\Delta t})(\mathbf{x},t)}{\mu^l}\mathbf{K}\Big(\nabla\Pi_{\mathcal{T},\Delta t}u_{\mathcal{D}}(\mathbf{x},t) - M^l\zeta^l\mathbf{g}\Big)\cdot\nabla_{\mathcal{D}_p}v_{\mathcal{D}}(\mathbf{x})d\mathbf{x}dt,
\end{aligned} \tag{31}$$

$$\begin{aligned}
B^n_{\mathcal{D}_g}(v_{\mathcal{D}}) &= \int_0^L \frac{1}{\alpha_g(x)}|S|\widetilde{\zeta^g}(\Pi_{\mathcal{D}_g}g(u_{\mathcal{D}}^n)(x))\nabla_{\mathcal{D}_g}g(u_{\mathcal{D}}^n)(x)\nabla_{\mathcal{D}_g}v_{\mathcal{D}}(x)dx\\
&= \frac{1}{\Delta t^n}\int_{t^{n-1}}^{t^n}\int_0^L \frac{1}{\alpha_g(x)}|S|\widetilde{\zeta^g}(p_{\mathcal{D}_g,\Delta t}(x,t))\partial_x\gamma\Pi_{\mathcal{T},\Delta t}g(u_{\mathcal{D}})(x,t)\nabla_{\mathcal{D}_g}v_{\mathcal{D}}(x)dxdt
\end{aligned} \tag{32}$$

and

$$C^n_{\mathcal{D}_p}(v_\mathcal{D}) = \frac{1}{\Delta t^n}\int_{t^{n-1}}^{t^n}\int_\Omega Q(\mathbf{x},t)\Pi_{\mathcal{D}_p}v_\mathcal{D}(\mathbf{x})d\mathbf{x}dt, \tag{33}$$

$$C^n_{\mathcal{D}_g}(v_\mathcal{D}) = \frac{1}{\Delta t^n}\int_{t^{n-1}}^{t^n}\int_0^L |S|q(x,t)\Pi_{\mathcal{D}_g}v_\mathcal{D}(x)dxdt, \tag{34}$$

in such a way that the system (25) is equivalent to: find $u_\mathcal{D} \in X_{\mathcal{D},\Delta t}$ with $u^n_\mathcal{D} - \bar{u}_\mathcal{D} \in X^0_\mathcal{D}$, $n = 1, \cdots, N$, such that

$$A^n_{\mathcal{D}_p}(v_\mathcal{D}) + A^n_{\mathcal{D}_g}(v_\mathcal{D}) + B^n_{\mathcal{D}_p}(v_\mathcal{D}) + B^n_{\mathcal{D}_g}(v_\mathcal{D}) = C^n_{\mathcal{D}_p}(v_\mathcal{D}) + C^n_{\mathcal{D}_g}(v_\mathcal{D}), \tag{35}$$

for all $v_\mathcal{D} \in X^0_\mathcal{D}$.

5.2.1 A priori estimates and existence of a discrete solution

Proposition 5.1 *There exists at least one solution $u_\mathcal{D} \in X_{\mathcal{D},\Delta t}$ to (25), and there exists a constant $C > 0$ depending only on the data, on $\theta_\mathcal{T}$, and on $\|\Pi_{\mathcal{D}_p}u^0_\mathcal{D}\|_{L^2(\Omega)}$, $\|\Pi_{\mathcal{D}_g}u^0_\mathcal{D}\|_{L^2(0,L)}$, $\|\Pi_\mathcal{T}\bar{u}_\mathcal{D}\|_V$ such that any solution $u_\mathcal{D} \in X_{\mathcal{D},\Delta t}$ to (25) satisfies*

$$\|\Pi_{\mathcal{D}_g,\Delta t}g(u_\mathcal{D})\|_{L^\infty(0,T;L^2(0,L))} + \|\nabla_{\mathcal{D}_p,\Delta t}u_\mathcal{D}\|_{L^2(0,T;L^2(\Omega))} + \|\nabla_{\mathcal{D}_g,\Delta t}g(u_\mathcal{D})\|_{L^2(0,T;L^2(0,L))} \le C. \tag{36}$$

Proof: We first prove the a priori estimate (36). Let us set $T_1 = \sum_{n=1}^N \Delta t^n A^n_{\mathcal{D}_p}(u^n_\mathcal{D})$, $T_2 = \sum_{n=1}^N \Delta t^n A^n_{\mathcal{D}_g}(u^n_\mathcal{D})$, $T_5 = \sum_{n=1}^N \Delta t^n A^n_{\mathcal{D}_p}(\bar{u}_\mathcal{D})$, $T_6 = \sum_{n=1}^N \Delta t^n A^n_{\mathcal{D}_g}(\bar{u}_\mathcal{D})$, $T_8 = \sum_{n=1}^N \Delta t^n (C^n_{\mathcal{D}_p}(u^n_\mathcal{D} - \bar{u}_\mathcal{D}) + C^n_{\mathcal{D}_g}(u^n_\mathcal{D} - \bar{u}_\mathcal{D}))$. We also define

$$T_3 = \sum_{n=1}^N \Delta t^n \int_\Omega \zeta^l \frac{k^l_r(\mathbf{x}, s^l(\mathbf{x}, \Pi_{\mathcal{D}_p}u^n_\mathcal{D}(\mathbf{x})))}{\mu^l}\mathbf{K}\nabla_{\mathcal{D}_p}(u^n_\mathcal{D} - \bar{u}_\mathcal{D})(\mathbf{x}) \cdot \nabla_{\mathcal{D}_p}(u^n_\mathcal{D} - \bar{u}_\mathcal{D})(\mathbf{x})\, d\mathbf{x}, \tag{37}$$

$$T_7 = \sum_{n=1}^N \Delta t^n \int_\Omega \zeta^l \frac{k^l_r(\mathbf{x}, s^l(\mathbf{x}, \Pi_{\mathcal{D}_p}u^n_\mathcal{D}(\mathbf{x})))}{\mu^l}\mathbf{K}\Big(M^l\zeta^l\mathbf{g} - \nabla_{\mathcal{D}_p}\bar{u}_\mathcal{D}(\mathbf{x})\Big) \cdot \nabla_{\mathcal{D}_p}(u^n_\mathcal{D} - \bar{u}_\mathcal{D})(\mathbf{x})d\mathbf{x}, \tag{38}$$

$$T_4 = \sum_{n=1}^N \Delta t^n \int_0^L \frac{1}{\alpha_g(x)}|S|\widetilde{\zeta^g}(\Pi_{\mathcal{D}_g}g(u^n_\mathcal{D})(x))\nabla_{\mathcal{D}_g}g(u^n_\mathcal{D})(x)\nabla_{\mathcal{D}_g}(u^n_\mathcal{D} - \bar{u}_\mathcal{D})(x)dx, \tag{39}$$

in such a way that

$$T_1 + T_2 + T_3 + T_4 = T_5 + T_6 + T_7 + T_8.$$

Accumulation terms: Firstly, using the assumption on s^l, the following estimate is a straightforward adaptation from Lemma 3.1 of [2].

$$T_1 \ge -\overline{\phi}\frac{\zeta^l L_s}{2}\|\Pi_{\mathcal{D}_p}u^0_\mathcal{D}\|^2_{L^2(\Omega)}. \tag{40}$$

Next, using $0 \le s^l(\mathbf{x}, u) \le 1$, we obtain the following estimate for T_5

$$T_5 \le \zeta^l\overline{\phi}\sqrt{|\Omega|}\|\Pi_{\mathcal{D}_p}\bar{u}_\mathcal{D}\|_{L^2(\Omega)}. \tag{41}$$

From (11), we have that

$$T_2 = \frac{|S|}{RT_e}\sum_{n=1}^N\sum_{m=1}^{m_x}|x_{m-\frac{1}{2}}x_{m+\frac{1}{2}}|(g(u^n_m) - g(u^{n-1}_m))u^n_m.$$

Using $G(u)=\displaystyle\int_0^u vg'(v)dv$ which verifies $G(b)-G(a)=b(g(b)-g(a))-\displaystyle\int_a^b(g(v)-g(a))dv$ and hence $b(g(b)-g(a))\geq G(b)-G(a)$ for all $(a,b)\in\mathbb{R}\times\mathbb{R}$, we obtain that

$$\begin{aligned}T_2&\geq\frac{|S|}{RT_e}\sum_{n=1}^{N}\sum_{m=1}^{m_x}|x_{m-\frac{1}{2}}x_{m+\frac{1}{2}}|(G(u_m^n)-G(u_m^{n-1})),\\&=\frac{|S|}{RT_e}\sum_{m=1}^{m_x}|x_{m-\frac{1}{2}}x_{m+\frac{1}{2}}|(G(u_m^N)-G(u_m^0)).\end{aligned}$$

Remark that $G(u)=\displaystyle\int_{g(0)}^{g(u)}g^{-1}(v)dv$, so that in view of assumption on g one has

$$\frac{\Big(g(u)-g(0)\Big)^2}{2\max_{v\in\mathbb{R}}g'(v)}\leq G(u)\leq\Big(\max_{v\in\mathbb{R}}g'(v)\Big)\frac{u^2}{2}.$$

Therefore

$$T_2\geq\frac{|S|}{2RT_e\max_{v\in\mathbb{R}}g'(v)}\Big(\|\Pi_{\mathcal{D}_g}g(u_{\mathcal{D}}^N)-g(0)\|_{L^2(0,L)}^2\Big)-\frac{|S|\max_{v\in\mathbb{R}}g'(v)}{2RT_e}\|\Pi_{\mathcal{D}_g}u_{\mathcal{D}}^0\|_{L^2(0,L)}^2.\tag{42}$$

Turning to T_6, we obtain the estimate

$$T_6\leq\frac{|S|}{RT_e}\|\Pi_{\mathcal{D}_g}\bar{u}_{\mathcal{D}}\|_{L^2(0,L)}\|\Pi_{\mathcal{D}_g}(g(u_{\mathcal{D}}^N)-g(u_{\mathcal{D}}^0))\|_{L^2(0,L)}.$$

We deduce that

$$T_6\leq\frac{|S|}{RT_e}\max\Big(\max_{v\in\mathbb{R}}g'(v),1\Big)\|\Pi_{\mathcal{D}_g}\bar{u}_{\mathcal{D}}\|_{L^2(0,L)}\Big(\|\Pi_{\mathcal{D}_g}g(u_{\mathcal{D}}^N)\|_{L^2(0,L)}+\|\Pi_{\mathcal{D}_g}u_{\mathcal{D}}^0\|_{L^2(0,L)}\Big).\tag{43}$$

Transport terms: Thanks to the assumptions on $\mathbf{K}$ and k_r^l we obtain the following estimates

$$T_3\geq\frac{\zeta^l}{\mu^l}k_{min}\underline{\lambda}\sum_{n=1}^{N}\Delta t^n\|\nabla_{\mathcal{D}_p}(u_{\mathcal{D}}^n-\bar{u}_{\mathcal{D}})\|_{L^2(\Omega)^3}^2\tag{44}$$

and

$$T_7\leq\frac{\zeta^l}{\mu^l}k_{max}\overline{\lambda}\sum_{n=1}^{N}\Delta t^n\|\nabla_{\mathcal{D}_p}(u_{\mathcal{D}}^n-\bar{u}_{\mathcal{D}})\|_{L^2(\Omega)^3}\Big(\|\nabla_{\mathcal{D}_p}\bar{u}_{\mathcal{D}}\|_{L^2(\Omega)^3}+M^l\zeta^l|\mathbf{g}|\sqrt{|\Omega|}\Big).\tag{45}$$

From (9) and (11), setting $b_{m,m+\frac{1}{2}}=\int_{x_m}^{x_{m+\frac{1}{2}}}\frac{dx}{\alpha_g(x)}$, $b_{m+1,m+\frac{1}{2}}=\int_{x_{m+\frac{1}{2}}}^{x_{m+1}}\frac{dx}{\alpha_g(x)}$ and

$$a_{m+\frac{1}{2}}=\frac{\widetilde{\zeta}^g(g(u_m^n))b_{m,m+\frac{1}{2}}+\widetilde{\zeta}^g(g(u_{m+1}^n))b_{m+1,m+\frac{1}{2}}}{|x_mx_{m+1}|},$$

for $m=0,\cdots,m_x$ we have that

$$\begin{aligned}T_4&=|S|\sum_{n=1}^{N}\Delta t^n\sum_{m=0}^{m_x}a_{m+\frac{1}{2}}\frac{(g(u_m^n)-g(u_{m+1}^n))(u_m^n-u_{m+1}^n)}{|x_mx_{m+1}|}\\&-|S|\sum_{n=1}^{N}\Delta t^n\sum_{m=0}^{m_x}a_{m+\frac{1}{2}}\frac{(g(u_m^n)-g(u_{m+1}^n))(\bar{u}_m-\bar{u}_{m+1})}{|x_mx_{m+1}|}.\end{aligned}$$

We deduce that

$$\begin{aligned} T_4 \geq\ & \frac{|S|}{\overline{\alpha}_g}\frac{\min_{v\in\mathbb{R}}\widetilde{\zeta}^g(v)}{\max_{v\in\mathbb{R}}g'(v)}\sum_{n=1}^{N}\Delta t^n\|\nabla_{\mathcal{D}_g}g(u_{\mathcal{D}}^n)\|_{L^2(0,L)}^2 \\ & -\frac{|S|}{\underline{\alpha}_g}\Big(\max_{v\in\mathbb{R}}\widetilde{\zeta}^g(v)\Big)\Big(\sum_{n=1}^{N}\Delta t^n\|\nabla_{\mathcal{D}_g}g(u_{\mathcal{D}}^n)\|_{L^2(0,L)}^2\Big)^{1/2}\Big(\sum_{n=1}^{N}\Delta t^n\|\nabla_{\mathcal{D}_g}\bar{u}_{\mathcal{D}}\|_{L^2(0,L)}^2\Big)^{1/2}. \end{aligned}$$

Using Young's inequality we obtain that

$$\begin{aligned} T_4 \geq\ & \frac{|S|}{2\overline{\alpha}_g}\frac{\min_{v\in\mathbb{R}}\widetilde{\zeta}^g(v)}{\max_{v\in\mathbb{R}}g'(v)}\sum_{n=1}^{N}\Delta t^n\|\nabla_{\mathcal{D}_g}g(u_{\mathcal{D}}^n)\|_{L^2(0,L)}^2 \\ & -\frac{|S|\overline{\alpha}_g}{2\underline{\alpha}_g}\frac{(\max_{v\in\mathbb{R}}g'(v))(\max_{v\in\mathbb{R}}\widetilde{\zeta}^g(v))}{\min_{v\in\mathbb{R}}\widetilde{\zeta}^g(v)}\sum_{n=1}^{N}\Delta t^n\|\nabla_{\mathcal{D}_g}\bar{u}_{\mathcal{D}}\|_{L^2(0,L)}^2. \end{aligned} \tag{46}$$

Using the discrete Poincaré inequalities of Lemma 5.2, we obtain the following estimate of the source terms

$$\begin{aligned} T_8 \leq\ & C_5\sum_{n=1}^{N}\Delta t^n\|\nabla_{\mathcal{D}_p}(u_{\mathcal{D}}^n-\bar{u}_{\mathcal{D}})\|_{L^2(\Omega)^3}\Big(\frac{1}{\Delta t^n}\int_{t^{n-1}}^{t^n}\|Q(.,t)\|_{L^2(\Omega)}dt\Big) \\ & +C_6|S|\sum_{n=1}^{N}\Delta t^n\|\nabla_{\mathcal{D}_g}(u_{\mathcal{D}}^n-\bar{u}_{\mathcal{D}})\|_{L^2(0,L)}\Big(\frac{1}{\Delta t^n}\int_{t^{n-1}}^{t^n}\|q(.,t)\|_{L^2(0,L)}dt\Big). \end{aligned} \tag{47}$$

Gathering the estimates (40),(42),(44), (46),(41),(43), (45), and (47), and using Young's and Cauchy-Schwarz inequalities, we conclude the proof of the a priori estimate (36).

To prove the existence of a solution $u_{\mathcal{D}}^n, n=1,\cdots,N$ to (25), let us consider the one parameter family of solutions obtained by setting $s^{l,\theta}(\mathbf{x},u)=\theta s^l(\mathbf{x},u)+1-\theta$, $\widetilde{\zeta}^{g,\theta}(p)=\theta\widetilde{\zeta^g}(p)+(1-\theta)\zeta_0^g$ with a given $\zeta_0^g>0$, and $g^\theta(u)=\theta g(u)+(1-\theta)u$. Let us remark that for all values of $\theta\in[0,1]$, the previous estimates still hold. Since for $\theta=0$, the system (25) becomes linear, it results that it admits a unique solution. By topological degree argument, we deduce the existence of at least one solution to (25) for $\theta=1$. □

5.2.2 Space and time translates estimates

The function space $L^2(\Omega)\times L^2(0,L)$ is equipped with the scalar product $\langle(u,p),(v,q)\rangle_{L^2(\Omega)\times L^2(0,L)}=\int_\Omega\zeta^l\phi uvd\mathbf{x}+\int_0^L\frac{|S|}{RT_e}pqdx$. For all $(u,p)\in L^2(\Omega)\times L^2(0,L)$ we also define the dual semi-norm $\|u\|_{-1,\mathcal{D}}$ by

$$\|(u,p)\|_{-1,\mathcal{D}}=\sup_{v_{\mathcal{D}}\in X_{\mathcal{D}}^0,v_{\mathcal{D}}\neq0}\frac{\langle(u,p),(\Pi_{\mathcal{D}_p}v_{\mathcal{D}},\Pi_{\mathcal{D}_g}v_{\mathcal{D}})\rangle_{L^2(\Omega)\times L^2(0,L)}}{\|\Pi_{\mathcal{T}}v_{\mathcal{D}}\|_V}. \tag{48}$$

Lemma 5.5 *There exists a constant $C>0$ depending only on the data, on $\theta_{\mathcal{T}}$, and on $\|\Pi_{\mathcal{D}_p}u_{\mathcal{D}}^0\|_{L^2(\Omega)}$, $\|\Pi_{\mathcal{D}_g}u_{\mathcal{D}}^0\|_{L^2(0,L)}$, $\|\Pi_{\mathcal{T}}\bar{u}_{\mathcal{D}}\|_V$ such that any solution $u_{\mathcal{D}}\in X_{\mathcal{D},\Delta t}$ to (25) satisfies the estimate*

$$\int_0^T\|\Big(\delta_{\mathcal{D}}s_{\mathcal{D}_p,\Delta t}^l(.,t),\delta_{\mathcal{D}}p_{\mathcal{D}_g,\Delta t}(.,t)\Big)\|_{-1,\mathcal{D}}^2dt\leq C. \tag{49}$$

Proof: Using (25), we obtain that for all $v_{\mathcal{D}} \in X^0_{\mathcal{D}}$

$$\begin{aligned}
&\langle\Big(\delta_{\mathcal{D}} s^l_{\mathcal{D}_p,\Delta t}(.,t^n), \delta_{\mathcal{D}} p_{\mathcal{D}_g,\Delta t}(.,t^n)\Big), (\Pi_{\mathcal{D}_p} v_{\mathcal{D}}, \Pi_{\mathcal{D}_g} v_{\mathcal{D}})\rangle_{L^2(\Omega)\times L^2(0,L)} = \\
&-\int_\Omega \zeta^l \frac{k^l_r(\mathbf{x}, s^l(\mathbf{x}, \Pi_{\mathcal{D}_p} u^n_{\mathcal{D}}(\mathbf{x})))}{\mu^l} \mathbf{K}(\nabla_{\mathcal{D}_p} u^n_{\mathcal{D}}(\mathbf{x}) - M^l \zeta^l \mathbf{g}) \cdot \nabla_{\mathcal{D}_p} v_{\mathcal{D}}(\mathbf{x}) d\mathbf{x} \\
&-\int_0^L \frac{1}{\alpha_g(x)} |S| \widetilde{\zeta}^g(\Pi_{\mathcal{D}_g} g(u^n_{\mathcal{D}})(x)) \nabla_{\mathcal{D}_g} g(u^n_{\mathcal{D}})(x) \nabla_{\mathcal{D}_g} v_{\mathcal{D}}(x) dx \\
&+\frac{1}{\Delta t^n} \int_{t^{n-1}}^{t^n} \Big(\int_\Omega Q(\mathbf{x},t) \Pi_{\mathcal{D}_p} v_{\mathcal{D}}(\mathbf{x}) d\mathbf{x} + \int_0^L |S| q(x,t) \Pi_{\mathcal{D}_g} v_{\mathcal{D}}(x) dx \Big) dt.
\end{aligned}$$

Using the discrete Poincaré inequalities of Lemma 5.2, and the assumption on the function g, we obtain the estimate

$$\begin{aligned}
&\langle\Big(\delta_{\mathcal{D}} s^l_{\mathcal{D}_p,\Delta t}(.,t^n), \delta_{\mathcal{D}} p_{\mathcal{D}_g,\Delta t}(.,t^n)\Big), (\Pi_{\mathcal{D}_p} v_{\mathcal{D}}, \Pi_{\mathcal{D}_g} v_{\mathcal{D}})\rangle_{L^2(\Omega)\times L^2(0,L)} \leq \\
&\zeta^l k_{max} \overline{\lambda} \Big(\|\nabla_{\mathcal{D}_p} u^n_{\mathcal{D}}\|_{L^2(\Omega)^3} + M^l \zeta^l |\mathbf{g}| \sqrt{|\Omega|} \Big) \|\nabla_{\mathcal{D}_p} v_{\mathcal{D}}\|_{L^2(\Omega)^3} \\
&+\frac{1}{\underline{\alpha}_g} |S| \Big(\max_{q\in\mathbb{R}} \widetilde{\zeta}^g(q) \Big) \|\nabla_{\mathcal{D}_g} g(u^n_{\mathcal{D}})\|_{L^2(0,L)} \|\nabla_{\mathcal{D}_g} v_{\mathcal{D}}\|_{L^2(0,L)} \\
&+C_5 \Big(\frac{1}{\Delta t^n} \int_{t^{n-1}}^{t^n} \|Q(.,t)\|_{L^2(\Omega)} dt \Big) \|\nabla_{\mathcal{D}_p} v_{\mathcal{D}}\|_{L^2(\Omega)^3} \\
&+C_6 |S| \Big(\frac{1}{\Delta t^n} \int_{t^{n-1}}^{t^n} \|q(.,t)\|_{L^2(0,L)} dt \Big) \|\nabla_{\mathcal{D}_g} v_{\mathcal{D}}\|_{L^2(0,L)}.
\end{aligned}$$

and the proof is achieved using Proposition 5.1 and the Cauchy-Schwarz inequality. □.

Lemma 5.6 *There exists a constant $C > 0$ depending only on the data, on $\theta_{\mathcal{T}}$, and on $\|\Pi_{\mathcal{D}_p} u^0_{\mathcal{D}}\|_{L^2(\Omega)}$, $\|\Pi_{\mathcal{D}_g} u^0_{\mathcal{D}}\|_{L^2(0,L)}$, $\|\Pi_{\mathcal{T}} \bar{u}_{\mathcal{D}}\|_V$ such that any solution $u_{\mathcal{D}} \in X_{\mathcal{D},\Delta t}$ to (25) satisfies the estimate for all $\tau \in \mathbb{R}$*

$$\begin{aligned}
&\int_{\mathbb{R}} \Big(\|s^l_{\mathcal{D}_p,\Delta t}(.,t+\tau) - s^l_{\mathcal{D}_p,\Delta t}(.,t)\|^2_{L^2(\Omega)} + \|p_{\mathcal{D}_g,\Delta t}(.,t+\tau) - p_{\mathcal{D}_g,\Delta t}(.,t)\|^2_{L^2(0,L)} \Big) dt \\
&\leq C\sqrt{|\tau|},
\end{aligned} \tag{50}$$

where $p_{\mathcal{D}_g,\Delta t}$ and $s^l_{\mathcal{D}_p,\Delta t}$ are extended by zero outside of respectively $(0,L)\times(0,T)$ and $\Omega\times(0,T)$.

Proof: From the Lipschitz assumptions on the functions s^l and g, and by definition of the semi-norm (48) we obtain the estimates

$$\begin{aligned}
&\int_\Omega \zeta^l \phi(\mathbf{x}) |s^l_{\mathcal{D}_p,\Delta t}(\mathbf{x},t+\tau) - s^l_{\mathcal{D}_p,\Delta t}(\mathbf{x},t)|^2 d\mathbf{x} + \int_0^L \frac{|S|}{RT_e} |p_{\mathcal{D}_g,\Delta t}(x,t+\tau) - p_{\mathcal{D}_g,\Delta t}(x,t)|^2 dx \\
&\leq L_{sp} \int_\Omega \zeta^l \phi(\mathbf{x}) (s^l_{\mathcal{D}_p,\Delta t}(\mathbf{x},t+\tau) - s^l_{\mathcal{D}_p,\Delta t}(\mathbf{x},t)) (\Pi_{\mathcal{D}_p,\Delta t} g(u_{\mathcal{D}})(\mathbf{x},t+\tau) - \Pi_{\mathcal{D}_p,\Delta t} g(u_{\mathcal{D}})(\mathbf{x},t)) d\mathbf{x} \\
&+\int_0^L \frac{|S|}{RT_e} (p_{\mathcal{D}_g,\Delta t}(x,t+\tau) - p_{\mathcal{D}_g,\Delta t}(x,t)) (\Pi_{\mathcal{D}_g,\Delta t} g(u_{\mathcal{D}})(x,t+\tau) - \Pi_{\mathcal{D}_g,\Delta t} g(u_{\mathcal{D}})(x,t)) dx \\
&\leq \max\Big(1, L_{Sp}\Big) \|s^l_{\mathcal{D}_p,\Delta t}(.,t+\tau) - s^l_{\mathcal{D}_p,\Delta t}(.,t), p_{\mathcal{D}_g,\Delta t}(.,t+\tau) - p_{\mathcal{D}_g,\Delta t}(.,t)\|_{-1,\mathcal{D}} \\
&\qquad \|\Pi_{\mathcal{T},\Delta t} g(u_{\mathcal{D}})(.,t+\tau) - \Pi_{\mathcal{T},\Delta t} g(u_{\mathcal{D}})(.,t)\|_V
\end{aligned}$$

Using Young's inequality, we obtain that there exists C such that for all $\tau \in (0,T)$

$$\begin{aligned}
&\int_0^{T-\tau} \Big(\|s^l_{\mathcal{D}_p,\Delta t}(.,t+\tau) - s^l_{\mathcal{D}_p,\Delta t}(.,t)\|_{L^2(\Omega)} + \|p_{\mathcal{D}_g,\Delta t}(.,t+\tau) - p_{\mathcal{D}_g,\Delta t}(.,t)\|_{L^2(0,L)} \Big) dt \\
&\leq \frac{C}{\sqrt{|\tau|}} \int_0^{T-\tau} \|s^l_{\mathcal{D}_p,\Delta t}(.,t+\tau) - s^l_{\mathcal{D}_p,\Delta t}(.,t), p_{\mathcal{D}_g,\Delta t}(.,t+\tau) - p_{\mathcal{D}_g,\Delta t}(.,t)\|_{-1,\mathcal{D}} dt \\
&+C\sqrt{|\tau|} \int_0^{T-\tau} \|\Pi_{\mathcal{T},\Delta t} g(u_{\mathcal{D}})(.,t+\tau) - \Pi_{\mathcal{T},\Delta t} g(u_{\mathcal{D}})(.,t)\|_V dt.
\end{aligned}$$

From BV properties of piecewise constant functions and from Lemma 5.5, we obtain that

$$\begin{aligned}
&\int_0^{T-\tau} \|s^l_{\mathcal{D}_p,\Delta t}(.,t+\tau) - s^l_{\mathcal{D}_p,\Delta t}(.,t), p_{\mathcal{D}_g,\Delta t}(.,t+\tau) - p_{\mathcal{D}_g,\Delta t}(.,t)\|_{-1,\mathcal{D}} dt \\
&\leq \tau \int_0^T \|\Big(\delta_{\mathcal{D}} s^l_{\mathcal{D}_p,\Delta t}(.,t), \delta_{\mathcal{D}} p_{\mathcal{D}_g,\Delta t}(.,t)\Big)\|_{-1,\mathcal{D}} dt \\
&\leq \tau\sqrt{T}\Big(\int_0^T \|\Big(\delta_{\mathcal{D}} s^l_{\mathcal{D}_p,\Delta t}(.,t), \delta_{\mathcal{D}} p_{\mathcal{D}_g,\Delta t}(.,t)\Big)\|^2_{-1,\mathcal{D}} dt\Big)^{1/2} \\
&\leq C\sqrt{T}\tau.
\end{aligned}$$

Using $0 \leq s^l(\mathbf{x}, v) \leq 1$ as well as the boundedness of $\|p_{\mathcal{D}_g,\Delta t}(.,t)\|_{L^2(0,L)}$ on $[0,T]$ from Proposition 5.1, we conclude the proof of Lemma 5.6. $\square$.

Lemma 5.7 *Let $\hat{p}_{\mathcal{D}} \in X_{\mathcal{D},\Delta t}$ be defined by $\hat{p}^n_{\mathcal{D}} = g(u^n_{\mathcal{D}}) - g(\bar{u}_{\mathcal{D}})$, we denote $\hat{p}_{\mathcal{D}_g,\Delta t} = \Pi_{\mathcal{D}_g,\Delta t}\hat{p}_{\mathcal{D}}$. There exists a constant $C > 0$ depending only on the data, on $\theta_{\mathcal{T}}$, and on $\|\Pi_{\mathcal{D}_p} u^0_{\mathcal{D}}\|_{L^2(\Omega)}$, $\|\Pi_{\mathcal{D}_g} u^0_{\mathcal{D}}\|_{L^2(0,L)}$, $\|\Pi_{\mathcal{T}}\bar{u}_{\mathcal{D}}\|_V$ such that any solution $u_{\mathcal{D}} \in X_{\mathcal{D},\Delta t}$ to (25) satisfies the following estimate for all $\xi \in \mathbb{R}^3$ and $\zeta \in \mathbb{R}$.*

$$\begin{aligned}
&\int_0^T \Big(\|s^l_{\mathcal{D}_p,\Delta t}(.+\xi,t) - s^l_{\mathcal{D}_p,\Delta t}(.,t)\|^2_{L^2(\mathbb{R}^3)} + \|\hat{p}_{\mathcal{D}_g,\Delta t}(.+\zeta,t) - \hat{p}_{\mathcal{D}_g,\Delta t}(.,t)\|^2_{L^2(\mathbb{R})}\Big) dt \\
&\leq C(|\xi| + |\zeta| + h_{\mathcal{T}})
\end{aligned} \tag{51}$$

where $s^l_{\mathcal{D}_p,\Delta t}$ and $\hat{p}_{\mathcal{D}_g,\Delta t}$ are extended on $\mathbb{R}^3$ (respectively on $\mathbb{R}$) by zero.

Proof: For any $\xi \in \mathbb{R}^3$ we define the set $\Omega_\xi = \bigcup_{j\in J}\{\mathbf{x} \in \Omega_j \mid \mathbf{x} + \xi \in \Omega_j\}$. From $\Pi_{\mathcal{T},\Delta t} u_{\mathcal{D}} \in L^2(0,T;H^1(\Omega))$ and $\gamma\Pi_{\mathcal{T},\Delta t}\hat{p}_{\mathcal{D}} \in L^2(0,T;H^1_0(0,L))$ and Proposition 5.1, it follows that there exists a constant C such that the following estimate holds for all $\xi \in \mathbb{R}^3$ and $\zeta \in \mathbb{R}$:

$$\begin{aligned}
&\int_0^T \Big(\|\Pi_{\mathcal{T},\Delta t} u_{\mathcal{D}}(.+\xi,t) - \Pi_{\mathcal{T},\Delta t} u_{\mathcal{D}}(.,t)\|^2_{L^2(\Omega_\xi)} + \|\gamma\Pi_{\mathcal{T},\Delta t}\hat{p}_{\mathcal{D}}(.+\zeta,t) - \gamma\Pi_{\mathcal{T},\Delta t}\hat{p}_{\mathcal{D}}(.,t)\|^2_{L^2(\mathbb{R})}\Big) dt \\
&\leq C(|\xi| + |\zeta|).
\end{aligned} \tag{52}$$

Combining the estimate (52) with Lemma 5.3 and Proposition 5.1, it results that there exists a constant C such that

$$\begin{aligned}
&\int_0^T \Big(\|\Pi_{\mathcal{D}_p,\Delta t} u_{\mathcal{D}}(.+\xi,t) - \Pi_{\mathcal{D}_p,\Delta t} u_{\mathcal{D}}(.,t)\|^2_{L^2(\Omega_\xi)} + \|\Pi_{\mathcal{D}_g,\Delta t}\hat{p}_{\mathcal{D}}(.+\zeta,t) - \Pi_{\mathcal{D}_g,\Delta t}\hat{p}_{\mathcal{D}}(.,t)\|^2_{L^2(\mathbb{R})}\Big) dt \\
&\leq C(|\xi| + |\zeta| + h_{\mathcal{T}}).
\end{aligned}$$

We conclude from the Lipschitz properties and the boundedness of s^l. $\square$.

5.2.3 Convergence

Lemma 5.8 *Let $(v^{(m)})_{m\in\mathbb{N}}$ be a sequence of functions in $L^2(0,T;U^0)$ such that there exists $C > 0$ with $\|v^{(m)}\|_{L^2(0,T;H^1(\Omega))} \leq C$. Then, there exists $v \in L^2(0,T;U^0)$ such that*

1. *up to a subsequence*

$$v^{(m)} \rightharpoonup v \quad in \quad L^2(\Omega\times(0,T)) \quad and \quad \nabla v^{(m)} \rightharpoonup \nabla v \quad in \quad L^2(\Omega\times(0,T))^3.$$

2. *up to the same subsequence*

$$\gamma v^{(m)} \rightharpoonup \gamma v \quad in \quad L^2((0,L)\times(0,T));$$

.

Proof: The proof of the first statement is classical, see e.g. the proof of Lemma 5.1 in [6]; moreover $v \in L^2(0,T;H^1_{\Gamma_D}(\Omega))$. Next, there exists $r \in L^2(0,T;L^2(0,L))$ such that $\gamma v^{(m)} \rightharpoonup r$ in $L^2(0,T;L^2(0,L))$. To conclude, let us prove that $\partial_s \gamma v = 0$ and $r = \gamma v$. For all $\varphi \in L^2((0,L)\times(0,T))$ and $\psi \in L^2(\partial S \times (0,T))$, there exist $\Psi \in L^2(0,T;H_{\rm div}(\Omega))$ such that $\Psi \cdot \mathbf{n} = \varphi(x,t)\psi(s,t)$ on Γ. Hence, one has

$$\int_0^T \int_\Omega (\nabla v^{(m)}(\mathbf{x},t)\cdot\Psi(\mathbf{x},t)+v^{(m)}(\mathbf{x},t){\rm div}\Psi(\mathbf{x},t))d\mathbf{x}dt-\int_0^T\int_0^L\int_{\partial S}(\gamma v^{(m)})(x,t)\varphi(x,t)\psi(s,t)dxdsdt = 0.$$

Passing to the limit in this equality one obtains that

$$\int_0^T \int_\Omega (\nabla v(\mathbf{x},t)\cdot\Psi(\mathbf{x},t)+v(\mathbf{x},t){\rm div}\Psi(\mathbf{x},t))d\mathbf{x}dt - \int_0^T\int_0^L\int_{\partial S} r(x,t)\varphi(x,t)\psi(s,t)dxdsdt = 0,$$

which implies that

$$\int_0^T\int_0^L\int_{\partial S}(\gamma v(x,s,t)-r(x,t))\varphi(x,t)\psi(s,t)dxdsdt = 0,$$

and hence that $\partial_s\gamma v = 0$ and $\gamma v = r$. $\square$.

Theorem 5.1 *Let $\mathcal{D}^{(m)}$,$\Delta t^{n,(m)}, n = 1,\cdots,N^{(m)}$, $m \in \mathbb{N}$ be a sequence of space time discretizations such that there exists $\theta > 0$ with $\theta_{\mathcal{T}^{(m)}} \le \theta$. It is assumed that $\lim_{m\to+\infty} h_{\mathcal{T}^{(m)}} = 0$, and that $\Delta t^{(m)} = \max_{n=1,\cdots,N^{(m)}} \Delta t^{n,(m)}$ tends to zero when $m \to +\infty$, and that $\|\Pi_{\mathcal{D}_p^{(m)}} u^0_{\mathcal{D}^{(m)}} - u_{init,p}\|_{L^2(\Omega)}$, $\|\Pi_{\mathcal{D}_g^{(m)}} u^0_{\mathcal{D}^{(m)}} - u_{init,g}\|_{L^2(0,L)}$, $\|\Pi_{\mathcal{T}^{(m)}}\bar{u}_{\mathcal{D}^{(m)}} - \bar{u}\|_V$ tends to zero when $m \to +\infty$. Then, there exist a subsequence of $m \in \mathbb{N}$ and a function $u \in L^2(0,T;V)$ solution of (23) such that up to this subsequence*

$$s^l_{\mathcal{D}_p^{(m)},\Delta t^{(m)}} \to s^l(.,u) \text{ strongly in } L^2(\Omega\times(0,T)),$$

$$\Pi_{\mathcal{D}_p^{(m)},\Delta t^{(m)}} u_{\mathcal{D}^{(m)}} \rightharpoonup u \text{ weakly in } L^2(\Omega\times(0,T)),$$

and

$$p_{\mathcal{D}_g^{(m)},\Delta t^{(m)}} \to g(\gamma u) \text{ strongly in } L^2((0,L)\times(0,T)).$$

Proof: From Proposition 5.1, Lemma 5.8, and the convergence to zero of $\|\Pi_{\mathcal{T}^{(m)}}\bar{u}_{\mathcal{D}^{(m)}} - \bar{u}\|_V$ we deduce that there exists $u \in L^2(0,T;U)$ with $u - \bar{u} \in L^2(0,T;U^0)$ such that up to a subsequence $\Pi_{\mathcal{T}^{(m)},\Delta t^{(m)}} u_{\mathcal{D}^{(m)}} \rightharpoonup u$ weakly in $L^2(\Omega\times(0,T))$, $\gamma\Pi_{\mathcal{T}^{(m)},\Delta t^{(m)}} u_{\mathcal{D}^{(m)}} \rightharpoonup \gamma u$ weakly in $L^2((0,L)\times(0,T))$, and $\nabla\Pi_{\mathcal{T}^{(m)},\Delta t^{(m)}} u_{\mathcal{D}^{(m)}} \rightharpoonup \nabla u$ weakly in $L^2(\Omega\times(0,T))^3$.

In view of Lemma 5.6, Lemma 5.7, and Lemma B.2 of [8], the Kolmogorov-Fréchet theorem implies that there exist two functions $s \in L^2(\Omega\times(0,T))$ and $\hat{p} \in L^2((0,L)\times(0,T))$ such that up to a subsequence $s^l_{\mathcal{D}_p^{(m)},\Delta t^{(m)}} \to S$ strongly in $L^2(\Omega\times(0,T))$ and $\hat{p}_{\mathcal{D}_g^{(m)},\Delta t^{(m)}} \to \hat{p}$ strongly in $L^2((0,L)\times(0,T))$. The sequence $\gamma\Pi_{\mathcal{T}^{(m)},\Delta t^{(m)}}\hat{p}_{\mathcal{D}^{(m)}}$ is uniformly bounded in $L^2(0,T;H^1_0(0,L))$, thus one can extract a subsequence of $\partial_x\gamma\Pi_{\mathcal{T}^{(m)},\Delta t^{(m)}}\hat{p}_{\mathcal{D}^{(m)}}$ weakly converging to some function $\hat{p}_x$ in $L^2((0,L)\times(0,T))$. Let $\varphi \in L^2(0,T;C^\infty_c(\mathbb{R}))$ and let $\gamma\Pi_{\mathcal{T}^{(m)},\Delta t^{(m)}}\hat{p}_{\mathcal{D}^{(m)}}$ be extended by zero outside of $(0,L)$, passing to the limit in

$$\int_0^T\int_{\mathbb{R}}\Big((\partial_x\gamma\Pi_{\mathcal{T}^{(m)},\Delta t^{(m)}}\hat{p}_{\mathcal{D}^{(m)}})\varphi(x,t)+\gamma\Pi_{\mathcal{T}^{(m)},\Delta t^{(m)}}\hat{p}_{\mathcal{D}^{(m)}}\partial_x\varphi(x,t)\Big)dxdt = 0,$$

we obtain that

$$\int_0^T\int_{\mathbb{R}}\Big(\hat{p}_x\varphi(x,t)+\hat{p}\partial_x\varphi(x,t)\Big)dxdt = 0,$$

and hence that $\hat{p}_x = \partial_x \hat{p}$ and $\hat{p} \in L^2(0,T;H_0^1(0,L))$. From the convergence to zero of $\|\Pi_{\mathcal{T}^{(m)}} \bar{u}_{\mathcal{D}^{(m)}} - \bar{u}\|_V$ and the assumptions on g we deduce that there exists $p \in L^2((0,L)\times(0,T))$ such that $p - g(\gamma \bar{u}) \in L^2(0,T;H_0^1(0,L))$ and such that $p_{\mathcal{D}_g^{(m)},\Delta t^{(m)}} \to p$ strongly and $\partial_x \gamma \Pi_{\mathcal{T}^{(m)},\Delta t^{(m)}} p_{\mathcal{D}^{(m)}}$ converges weakly to $\partial_x p$ up to subsequence. Using the Minty's trick stated in Lemma 3.6 of [2] one can show that $s = s^l(.,u)$ and $p = g(\gamma u)$.

It remains to show that u is a solution to (23). We will drop the superscript (m) in the following for the sake of convenience. Let $\mathcal{C}(\Omega \times [0,T))$ be the subspace of functions φ of $C^\infty\Big(\overline{\Omega} \times [0,T]\Big)$ vanishing at $t = T$ and on Γ_D and such that $\partial_s \varphi = 0$ on Γ. Then, let $\psi \in \mathcal{C}(\Omega \times [0,T))$ and consider the function $\overline{\psi}(t) = P_{\mathcal{D}} \psi(.,t) \in X_{\mathcal{D}}^0$.

Next, setting $v_{\mathcal{D}} = \overline{\psi}(t^{n-1})$ in (35), multiplying the left and right hand sides by Δt^n and summing over n, we obtain that

$$\sum_{n=1}^{N} \Delta t^n \Big(A_{\mathcal{D}_p}^n(\overline{\psi}(t^{n-1})) + A_{\mathcal{D}_g}^n(\overline{\psi}(t^{n-1})) + B_{\mathcal{D}_p}^n(\overline{\psi}(t^{n-1})) + B_{\mathcal{D}_g}^n(\overline{\psi}(t^{n-1})) \Big) = C_{\mathcal{D}_p}^n(\overline{\psi}(t^{n-1})) + C_{\mathcal{D}_g}^n(\overline{\psi}(t^{n-1})).$$

First, using the chain rule and $\overline{\psi}(T) = 0$, we have that

$$\begin{aligned} \sum_{n=1}^{N} \Delta t^n A_{\mathcal{D}_p}^n(\overline{\psi}(t^{n-1})) = & -\sum_{n=1}^{N} \int_{t^{n-1}}^{t^n} \int_\Omega \zeta^l \phi(\mathbf{x}) s_{\mathcal{D}_p,\Delta t}^l(\mathbf{x},t) \partial_t \Pi_{\mathcal{D}_p} \overline{\psi}(t)(\mathbf{x}) d\mathbf{x} dt \\ & + \int_\Omega \zeta^l \phi(\mathbf{x}) s^l(\mathbf{x}, \Pi_{\mathcal{D}_p} u_{\mathcal{D}}^0(\mathbf{x})) \Pi_{\mathcal{D}_p} \overline{\psi}(0)(\mathbf{x}) d\mathbf{x}. \end{aligned}$$

We deduce from the strong convergence of $s_{\mathcal{D}_p,\Delta t}^l$ to $s^l(.,u)$, the strong convergence of $\Pi_{\mathcal{D}_p} u_{\mathcal{D}}^0$ to $u_{init,p}$, and the regularity of ψ, that

$$\begin{aligned} \sum_{n=1}^{N} \Delta t^n A_{\mathcal{D}_p}^n(\overline{\psi}(t^{n-1})) \to & -\int_0^T \int_\Omega \zeta^l \phi(\mathbf{x}) s^l(\mathbf{x}, u(\mathbf{x},t)) \partial_t \psi(\mathbf{x},t) d\mathbf{x} dt \\ & + \int_\Omega \zeta^l \phi(\mathbf{x}) s^l(\mathbf{x}, u_{init,p}(\mathbf{x})) \psi(\mathbf{x},0) d\mathbf{x}. \end{aligned}$$

Similarly, we have that

$$\begin{aligned} \sum_{n=1}^{N} \Delta t^n A_{\mathcal{D}_g}^n(\overline{\psi}(t^{n-1})) = & -\sum_{n=1}^{N} \int_{t^{n-1}}^{t^n} \int_0^L \frac{|S|}{RT_e} p_{\mathcal{D}_g,\Delta t}(x,t) \partial_t \Pi_{\mathcal{D}_g} \overline{\psi}(t)(x) dx dt \\ & + \int_0^L \frac{|S|}{RT_e} g(\Pi_{\mathcal{D}_g} u_{\mathcal{D}}^0(x)) \Pi_{\mathcal{D}_g} \overline{\psi}(0)(x) dx. \end{aligned}$$

We deduce from the strong convergence of $p_{\mathcal{D}_g,\Delta t}$ to $g(\gamma u)$, the strong convergence of $\Pi_{\mathcal{D}_p} u_{\mathcal{D}}^0$ to $u_{init,g}$, and the regularity of ψ, that

$$\begin{aligned} \sum_{n=1}^{N} \Delta t^n A_{\mathcal{D}_g}^n(\overline{\psi}(t^{n-1})) = & -\int_O^T \int_0^L \frac{|S|}{RT_e} g(\gamma u)(x,t) \partial_t \gamma \psi(x,t) dx dt \\ & + \int_0^L \frac{|S|}{RT_e} g(u_{init,g})(x) \gamma \psi(x,0) dx. \end{aligned}$$

Turning to the diffusion terms, we have from the weak convergence of $\nabla \Pi_{\mathcal{T},\Delta t} u_{\mathcal{D}}$ to ∇u, the strong convergence of $s_{\mathcal{D}_p,\Delta t}^l$ to $s^l(.,u)$, the assumption on k_r^l, and the regularity of ψ, that

$$\sum_{n=1}^{N} \Delta t^n B_{\mathcal{D}_p}^n(\overline{\psi}(t^{n-1})) \to \int_0^T \int_\Omega \zeta^l \frac{k_r^l(\mathbf{x}, s^l(\mathbf{x}, u(\mathbf{x},t)))}{\mu^l} \mathbf{K}(\nabla u(\mathbf{x},t) - M^l \zeta^l \mathbf{g}) \cdot \nabla \psi(\mathbf{x},t) d\mathbf{x} dt$$

Similarly, we deduce from the weak convergence of $\partial_x \gamma \Pi_{\mathcal{T},\Delta t} u_{\mathcal{D}}$ to $\partial_x g(\gamma u)$, the strong convergence of $p_{\mathcal{D}_g,\Delta t}$ to $g(\gamma u)$, the assumption on $\widetilde{\zeta^g}$, and the regularity of ψ, that

$$\sum_{n=1}^{N} \Delta t^n B^n_{\mathcal{D}_g}(\overline{\psi}(t^{n-1})) \to \int_0^T \int_0^L \frac{1}{\alpha_g(x)} |S| \widetilde{\zeta^g}(g(\gamma u)(x,t)) \partial_x g(\gamma u)(x,t) \partial_x \gamma \psi(x,t) dx dt.$$

Turning to the source terms, from the regularity of ψ, we obtain that

$$\sum_{n=1}^{N} \Delta t^n \Big(C^n_{\mathcal{D}_p}(\overline{\psi}(t^{n-1})) + C^n_{\mathcal{D}_g}(\overline{\psi}(t^{n-1})) \Big) \to \int_0^T \int_\Omega Q(\mathbf{x},t)\psi(\mathbf{x},t) d\mathbf{x} dt + \int_0^T \int_0^L |S| q(x,t) \gamma \psi(x,t) dx dt.$$

6 Conclusion

A reduced model coupling the 3D gas liquid compositional Darcy flow in a porous media and a 1D compositional gas free flow has been proposed and applied to predict the mass exchanges occurring at the interface between the repository and the ventilation excavated galleries. The model takes into account the low permeability of the disposal to simplify the coupling conditions and uses a No Pressure Wave approximation in the free flow domain. The VAG scheme has been extended to the discretization of such model. It has the advantage compared with classical CVFE approaches to avoid in a natural way the mixing of the porous and free media properties inside the control volumes at the nodes located at the interface. The discretization has been validated using a quasi analytical solution for the stationary state which is shown to provide a very good approximation of the converged numerical solution of the coupled model. Finally, the convergence of the VAG discretization to a weak solution has been proved for a simplified model coupling the 3D Richards approximation for the liquid pressure in the porous medium and the Darcy approximation of the 1D gas pressure equation in the gallery. In [19], the reduced model of subsection 4.3 is compared with a full dimensional model using the Reynolds-averaged Navier-Stokes equations combined with an algebraic turbulent model in the gallery. The numerical results, using a boundary layer thickness δ computed from a diagonal approximation of the Steklov Poincaré operator related to the convection diffusion equation in the gallery for the water component, exhibit a very good match between both models.

References

[1] R. Eymard, C. Guichard, R. Herbin, Small-stencil 3d schemes for diffusive flows in porous media. ESAIM: Mathematical Modelling and Numerical Analysis, **46**, 265-290 (2010)

[2] R. Eymard, C. Guichard, R. Herbin, R. Masson, Gradient schemes for two-phase flow in heterogeneous porous media and Richards equation. ZAMM - Journal of Applied Mathematics and Mechanics **94** 7,8, 560-585 (2014).

[3] R. Eymard, R. Herbin, C. Guichard, R. Masson, Vertex centred discretization of compositional multiphase Darcy flows on general meshes. Comp. Geosciences, **16**, 987-1005 (2012)

[4] R. Masson, L. Trenty, Y. Zhang, Formulations of two-phase liquid gas compositional Darcy flows with phase transitions. International Journal of Finite Volume (2014).

[5] K. Mosthaf, K. Baber, B. Flemisch, R. Helmig, A. Leijnse, I. Rybak,B. Wohlmuth, A coupling concept for two-phase compositional porous-medium and single-phase compositional free flow. Water Resources Research **47**(10) (2011)

[6] K. Brenner, M. Groza, C. Guichard, R. Masson, Vertex approximate gradient scheme for hybrid dimensional two-phase darcy flows in fractured porous media. ESAIM: M2AN **49** 303-330 (2015).

[7] K. Brenner, R. Masson, Convergence of a vertex centred discretization of two-phase darcy flows on general meshes. International Journal of Finite Volume, **june** (2013)

[8] R. Eymard, P. Féron, T. Gallouët, C. Guichard, R. Herbin, Gradient schemes for the stefan problem. IJFV - International Journal on Finite Volumes, **june** (2013).

[9] A. Bourgeat, M. Jurak, F. Smai, Two phase partially miscible flow and transport in porous media; application to gas migration in nuclear waste repository. Computational Geosciences, **13**(1), 29-42 (2009).

[10] O. Angelini, C. Chavant, E. Chénier, R. Eymard, S. Granet, Finite volume approximation of a diffusion-dissolution model and application to nuclear waste storage. Mathematics and Computers in Simulation, **81**(10), 2001-2017 (2011).

[11] R. Helmig, B. Flemisch, M. Wolff, A. Ebigbo, H. Class, Model coupling for multiphase flow in porous media. Advances in Water Resources, **51** (2013).

[12] M. Discacciati, E. Miglio, A. Quarteroni, Mathematical and numerical models for coupling surface and groundwater flows. Appl. Num. Math., **43** (2002).

[13] V. Girault, B. Rivière, DG approximation of coupled Navier-Stokes and Darcy equations by beaver-joseph-saffman interface condition. SIAM J. Numer. Anal., **47** (2009).

[14] K. Baber, K. Mosthaf, B. Flemisch, R. Helmig, S. Müthing, Numerical scheme for coupling two-phase compositional porous-media flow and one-phase compositional free flow. IMA Journal of Applied Mathematics, **77**(6) (2012).

[15] K. Mosthaf, Modeling and Analysis of Coupled Porous-Medium and Free Flow with Application to Evaporation Processes. PhD Thesis, University of Stuttgart, 2013.

[16] A. Lauser, C. Hager, R. Helmig, B. Wohlmuth, A new approach for phase transitions in miscible multi-phase flow in porous media, Advances in Water Resources 34, pp. 957-966, 2011.

[17] Q. H. Tran, D. Ferre, C. Pauchon and J. P. Masella, Transient Simulation of Two-Phase Flows in Pipes. Oil & Gas Science and Technology, **53**(6), 801-811 (1998).

[18] A. D. Ventcel. On boundary conditions for multi-dimensional diffusion processes. Theor. Probability Appl., 4:164-177, 1959.

[19] Y. Zhang, Modélisation et simulation des dispositifs de ventilation dans les stockages de déchets radioactifs, PhD thesis, december 2015.